University of Nottingham
UK | CHINA | MALAYSIA

# Analysis of the Earth-Moon Lagrange Points for Improving GNSS Performance in Lunar Space

MRes Thesis

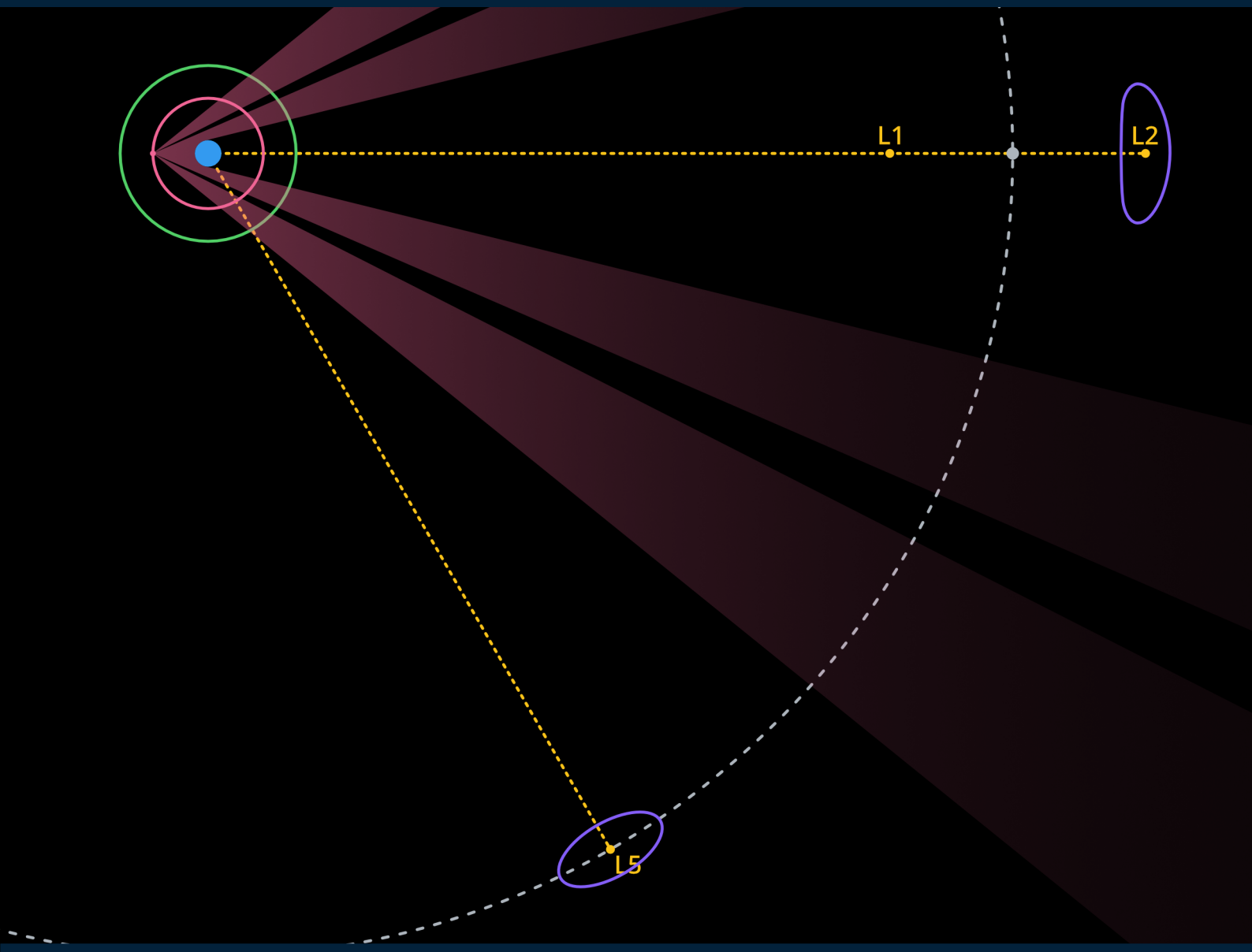


**Luis Cormier**
August 2023

# Contents

# List of Acronyms & Abbreviations

| | |
|---|---|
| ASI | Italian Space Agency (Agenzia Spaziale Italiana) |
| CR3BP | Circular Restricted Three-Body Problem |
| DOP | Dilution of Precision |
| ECEF | Earth-Centred Earth-Fixed |
| ESA | European Space Agency |
| GEO | Geostationary Orbit |
| GDOP | Geometric Dilution of Precision |
| GMAT | General Mission Analysis Tool |
| GNSS | Global Navigation Satellite System |
| GPS | Global Positioning System |
| HEO | High-Earth Orbit |
| $L_n$ | Lagrange Point $n$ |
| LEO | Low-Earth Orbit |
| LO | Lunar Orbit |
| MCMF | Moon-Centred Moon-Fixed |
| MEO | Medium-Earth Orbit |
| NASA | National Aeronautics and Space Administration |
| NGI | Nottingham Geospatial Institute |
| NRHO | Near-Rectilinear Halo Orbit |
| PNT | Position, Navigation, and Timing |
| RF | Radio Frequency |
| SSV | Space Service Volume |
| UKSA | United Kingdom Space Agency |

# List of Figures

# List of Tables

# 1 Introduction

This dissertation discusses the potential use of the Earth-Moon Lagrange points for improving global navigation satellite system (GNSS) signal availability and distribution on Lunar missions. The Lagrange points are points of equilibrium which occur when modelling the Earth and Moon under the circular restricted three body problem (CR3BP), and represent interesting yet sparsely research potential for Lunar missions. This chapter provides an overview of the project, while Chapter 2 discusses an overview of key literature in the field of positioning around the Moon, as well as some alternative proposals. The methodology used throughout this project is described in Chapter 3, with key results presented in Chapter 4 and their implications discussed. Chapter 5 talks about the implications of this research, and the factors which could affect its practical roll-out in real missions. Finally, a summary of the whole project is provided in Chapter 6.

## 1.1 Background

Despite the first spacecraft reaching the Moon in 1959, space agencies from around the world continue to explore our nearest celestial neighbour. In August 2023 alone, two missions aimed to land a spacecraft in the south pole region - a task which had not previously been achieved. Of those two missions, one successfully landed, while the other experienced an anomaly which is thought to have resulted in it crashing into the surface. At the time of writing, no formal investigation has concluded the cause. Over half a century since the last crewed landing on the Moon, the Artemis programme is once again preparing to send humans to the surface, with a new space station in Lunar orbit planned to expand experimental opportunities in Lunar space. As mission complexity increases, technological demands for the supporting infrastructure increase, especially in safety-critical applications in which errors can cause the loss of spacecraft, or life. One key area of interest is the development of reliable communications and navigation infrastructure, to support the ever-increasing manifest of missions to the Moon in the coming years. The European Space Agency aims to develop this infrastructure ready for its missions to the Moon, and the United Kingdom is a major investor in technologies to support this endeavour (UK Space Agency 2023), with over £50m in funding available in 2023 alone to support research into this growing area.

Tentatively scheduled for launch in 2023, the LuGRE mission aims to be the first to obtain GNSS signals from the Lunar surface (Parker et al. 2022), providing *in situ* reference data for this problem for the first time. The mission represents a key step towards achieving accurate positioning beyond Earth orbit, and will be the first step in determining the feasibility of GNSS as a technology in Lunar missions. Jointly developed by the National Aeronautics and Space Administration (NASA) and the Italian Space Agency (ASI), LuGRE will collect GNSS measurements throughout its journey to the Moon, and from its final landing site on the surface, and will make this data openly available to researchers in this field.

As discussed in Section 2.2, the use of GNSS outside the standard space service volume (SSV) has yet to be proven at distances as far as the Moon, however experimental data has shown promising results for its performance. However, its ability to pinpoint a receiver's location is limited by its visibility with Earth, and the quality of the solution is affected by the distribution of signal sources available to a receiver. While different approaches to improve this coverage and quality have been proposed in the past, this research will investigate the potential of using stable equilibrium points for improving GNSS performance - an area which has received relatively little attention to date.

## 1.2 Aims and Objectives

### 1.2.1 Research Aim

The purpose of this research project was to analyse the use of GNSS augmentation satellites at the Earth-Moon Lagrange points, specifically $L_2$, $L_4$, and $L_5$, and determine the change in performance and signal quality these augmentation satellites would bring to an autonomous GNSS receiver in Lunar space.

### 1.2.2 Primary Objectives

Throughout this research, the primary objectives of the project were as follows:

1. Review major upcoming missions to the Moon and beyond, to identify key requirements for PNT
2. Assess the current simulation processes for deep space satellite constellations and GNSS
3. Develop simulation methods for modelling GNSS availability with and without augmentations
4. Analyse the effects of augmenting GNSS with satellites at $L_2$, $L_4$, and $L_5$
5. Evaluate the relative performance of the proposed solution, and their long-term suitability for representative case studies

# 2 Literature Review

Since the introduction of the first Global Positioning System (GPS) satellites from the United States launched 45 years ago, research into applications of the technology behind the system expanded greatly following its demilitarisation in the 1980s. While GPS, and the other international networks that followed it, mainly focused on terrestrial use, space-based applications have long been a key area of interest - with satellite tracking provided as one of three examples of benefits of GPS in space in a press release issued by the Office of the United States Secretary of Commerce (2000) following the discontinuation of selective availability. In the past two decades, with public access to the GPS network opened up, combined with additional GNSS constellations from China and the European Union, researchers have attempted to identify the practical limits of GNSS in space, and methods for overcoming these limits on future missions the the Moon. This chapter aims to summarise a number of key areas of prior research, and identify key questions which remain.

## 2.1 Standalone Lunar Constellations

Traditional proposals for the development of a Lunar positioning system involve the creation of a standalone GNSS constellation around the Moon, similar in designs to the ones around the Earth. Constellations such as this can in theory be applied to any celestial body, to provide positioning and navigation abilities in the vicinity. While a network of dozens of full-size GNSS satellites around the Moon would be a large expense to any agency setting out to achieve autonomous positioning, the miniaturisation of space technology in recent decades has led to opportunities for smaller, cheaper missions. Wijnen et al. (2018) proposed the use of 28 3U-sized CubeSats deployed in three planes around the Moon, which collectively were able to provide a standalone positioning system akin to those used on Earth. Their study focused on the use of novel electric propulsion methods to achieve stationkeeping in a system small enough to fit within a standard size CubeSat, although analysis of constellation design to ensure a minimum visibility of four satellites was maintained across the Lunar surface was performed. While significantly cheaper to implement than a traditional GNSS network, Wijnen et al. estimated a minimum cost of US$31m to develop and launch the system, although a practical deployment of a CubeSat-based GNSS system would likely cost significantly more, to ensure redundancy within the system and long-term survivability, especially in a class of satellites with a nominal lifespan of a few years.

The design of a constellation is key when developing a standalone positioning network, with small differences in conditions resulting in large changes to the performance. Analysis performed by Arcia Gil et al. (2023) investigated over 12000 unique constellation designs of varying parameters, and isolated the ten which provided the best performance for a Lunar GNSS system. Compared to reference orbits in relevant literature, the ten constellations proposed by Arcia Gil et al. experienced a 44% improvement in performance.

To reduce complexity, frozen orbits have been proposed as an alternative to traditional constellations. Shirobokov, Trofimov, and Ovchinnikov (2021) investigated the use of such orbits to deploy a stable, minimal-maintenance network to provide positioning services for Lunar missions using a constellation of small satellites equipped with low-gain omnidirectional antennas. Their analysis suggested 300 of these satellites would be required to provide continuous, redundant coverage across the whole Lunar surface, however this could be reduced to as low as 100 satellites if interest were focused at the polar regions. The optimal design of frozen orbits for a given target is a key problem, which Trofimov, Shirobokov, and Ovchinnikov (2022) present modelling methods for.

On the other end of the scale, a minimal satellite configuration using frozen orbits is also presented by Jun et al. (2022), in which only two satellites are used to provide accurate positioning via Doppler ranging for a specific region on the Lunar surface. A key concept of their proposal is the ability to use any orbiting satellite for Doppler ranging, including spacecraft which travelled together to reach the celestial body. For example, on the Cassini–Huygens, the orbit of Cassini could have been used by the Hygens lander to determine its relative position, without any additional prior infrastructure required.

## 2.2 Direct Side-Lobe Signals

Due to the design of GNSS satellites, the majority of their signal is directed towards the Earth in the primary beam of the antenna, which has a half beam width of approximately $23.5°$. However, the antenna patterns used on most terrestrial GNSS satellites also gives rise to a weaker side beam, between $27°$ and $39°$ offset, which extends out into space beyond the Earth. The use of these side-lobe signals has been proposed for use in Lunar missions, and has been experimentally proven at shorter distances.

The use of side lobe signals for Lunar missions has been extensively analysed for a variety of missions by Delépaut, Schönfeldt, et al. (2019), in which mean visibility was suggested to be near 100% in their modelling. This study in particular included detailed maps of antenna patterns currently in use on GPS and Galileo satellites, which were used to accurately model signal characteristics of each GNSS satellite and determine their visibility from the Moon. The same team continues to publish similar studies into the use of side-lobe signals for Lunar GNSS (Delépaut, Giordano, et al. 2020).

As signals from side lobes are weaker than the primary GNSS lobe, and are received at a much greater distance, specialised hardware is likely to be required in order to utilise these signals around the Moon. Work done by Musumeci et al. (2016) into the design of a weak GNSS signal receiver suggest signals with a noise density ratio as low as 5-8 dB-Hz could be decoded, providing a positional accuracy in the order of 50-100 metres.

Side-lobe GNSS signals present the potential for continuous coverage across the whole trajectory from the Earth to the Moon, with Guan et al. (2022) publishing a study into the use of side-lobe signals from GPS, Galileo, GLONASS, and BeiDou, for positioning in geostationary orbit (GEO), high-Earth orbit (HEO), and Lunar orbit. While the authors noted promising positioning accuracy of approximately $20\,\mathrm{m}$ in GEO and HEO, they noted an improved receiver sensitivity was required to achieve similar results from Lunar distances.

While side-lobe signals have not yet been proven at distances as far as the Moon, their use has been proposed for use on missions closer to Earth, with satellites in geostationary orbit being a key interest. Ji, Kwon, and Won (2021) discusses the use of side-lobe signals for orbit determination of satellites over the Korean peninsula. Through their analysis, they determined the geometric dilution of precision (GDOP) achieved in GEO using solely main lobe signals could be improved by an order of magnitude with the addition of side-lobe signals, bringing it down to an average of 9.94, within the acceptable range for positioning. Prior work by Ji, Shin, and Won (2021) noted the decrease in signal-to-noise ratio of the side lobe signals, which limits their helpfulness in improving GNSS performance. Similar studies into side-lobe GNSS signals for GEO satellites have been performed by Konin and Shyshkov (2016) using the GPS and GLONASS constellations.

GNSS positioning using main- and side-lobes has been experimentally proven on the MMS mission, which was able to decode GNSS signals and provide a position fix at an altitude of $190\,000\,\mathrm{km}$ above the Earth (Winternitz et al. 2017), almost 54% of the way to the Moon. This practical achievement of high-altitude GNSS outside

of the standard space service volume proves the potential for using GNSS in Lunar space.

## 2.3 Spacecraft at Lagrange Points

When modelling the Earth-Moon system without including external sources of gravity from bodies such as the Sun or Jupiter, the model can be simplified to the Circular Restricted Three Body Problem (CR3BP, or sometimes CRTBP). In this model, the third body, usually a satellite, is assumed to have a negligible mass compared to the two primary bodies, which both orbit around their common barycentre. When restricting the motion of the three bodies to this circular problem, five points of equilibrium arise in which relative stability can be achieved, commonly referred to as Lagrange points.

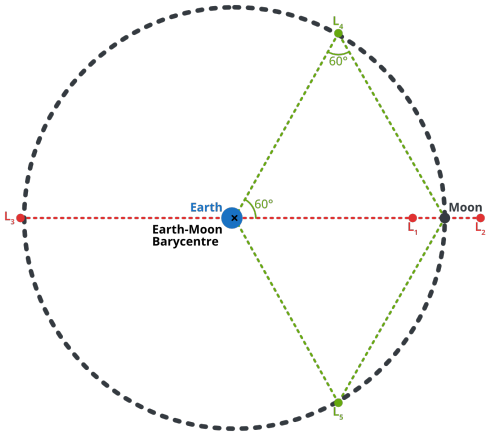


Figure 2.1: Location of the five equilibrium points in the Earth-Moon system

Three of these lie on the colinear axis between the two major bodies, in this case the Earth and the Moon. Discovered by Euler (1767), these colinear points lie partway between the Earth and the Moon ($L_1$), at a point in space perpetually "behind" the Moon ($L_2$), and at a point in conjunction with the Moon on the opposite side of the Earth ($L_3$). These three points are shown in red in Figure 2.1, note the $L_3$ point lies slightly beyond the orbit of the Moon. All three of these points are nominally unstable, with objects at the three points gradually drifting away over time due to orbital perturbations, however with minimal stationkeeping it is possible to be in a periodic orbit which appears to follow the three Lagrange points.

The other two Lagrange points were discovered by Lagrange (1867), and are located in a triangular configuration with respect to the two bodies. Taking the Earth and the Moon as one side of an equilateral triangle, the $L_4$ and $L_5$ points are situated at the third vertex, exactly $60°$ ahead and behind the Moon, slightly outside of its orbit, as shown in green in Figure 2.1. In contrast to the colinear points, these triangular points are nominally stable, and any perturbations from this orbit will be counteracted by the gravitational forces of the two major bodies, causing the spacecraft to orbit the point perpetually (in an ideal model).

With the Moon being tidally locked to the Earth, this means the orbital period and rotational period of the Moon are approximately equal, resulting in the same side of the Moon facing the Earth at all times. As all five equilibrium points are fixed in the Earth-Moon rotating frame, the practical effect of placing a satellite near any of these points will result in it appearing fixed in space from a ground observer, with only a slight change in position due to the libration of the Moon.

### 2.3.1 Unstable Colinear Points

Despite being nominally unstable, the $L_1$ and $L_2$ points are a popular location for spacecraft to be placed, due to the benefits these points present with respect to orbital geometry. Outside of GNSS, the much-publicised James Webb Space Telescope was positioned in a halo orbit around the Sun-Earth $L_2$ point, to minimise infrared interference from the Sun and Earth, while being able to remain in that position with minimal stationkeeping requirements.

One of the earliest investigations into the use of the colinear Lagrange points for navigation in Lunar space came from Carpenter et al. (2004), who discussed the use of a satellite at the $L_2$ point. In this paper, it was proposed the GPS measurements be augmented with a one-way Doppler ranging technique from the $L_2$ satellite, reducing the potential signal complexity of the augmentation system. The research suggested a potential position and velocity accuracy better than $1\,\mathrm{km}$ and $5\,\mathrm{cm}\cdot\mathrm{s}^{-1}$ respectively, which they note is a promising improvement compared to the existing methods of positioning in missions up to the time of publication. Carpenter et al. also discussed the implications of placing a similar satellite near the $L_1$ point, discussing its potential for use in the transfer phase of a Lunar mission.

Following on from this, a PhD thesis by Hill (2007) also investigated the use of a single spacecraft at the colinear Lagrange points for direct satellite-to-satellite positioning, also using techniques such as Doppler ranging. Their results suggest a positioning error in the order of $100\,\mathrm{m}$, even with the inclusion of simulated gravitational and weather-related errors. Critically, Hill noted that the operational costs of installing and maintaining a Lunar positioning system using static satellites at equilibrium points can be far lower than alternatives such as a full constellation in Lunar orbit. As most missions to the Moon are taxpayer-funded government agency missions, the reduced infrastructure cost to create a navigation system in this way can be appealing, especially as the same infrastructure can be used to support communications between Earth and Moon-based spacecraft.

While methods focused around Doppler ranging can significantly reduce cost and complexity of a Lunar positioning system, due to the reduced number of satellites required, it does give rise to greater uncertainties due to a reciever's position being calculated from a single point in space. While both Hill and Carpenter et al. have shown promising results, the lack of redundancy in the system, combined with alternative methods proposed since these publications, suggests a Doppler-based system may be insufficient for modern uses. However, the technology could be implemented as a secondary form of low-accuracy positioning, both as a backup system in case the primary method fails, or as a way of determining approximate positioning from a "cold" startup condition.

In contrast to using Doppler ranging as the main positioning method, Romagnoli and Circi (2010) proposed a constellation of four satellites at each of the $L_1$ and $L_2$ points, each $90°$ out of phase with each other. Notably, this network differs from the ones discussed by Hill and Carpenter et al., as it aims to provide standalone positioning without using the terrestrial GNSS network. Accurate baseline positioning of the eight satellites near the Lagrange points could be obtained using laser ranging, either from Earth (except for when $L_2$ satellites are occluded by the Moon), or static ground stations on the Lunar surface - such as a potential crewed base. Due to the tidal locking of the Moon, each hemisphere of the Moon would only ever be serviced by one of the two constellations, with four satellites in each hemisphere being used to ensure the minimum required number of pseudo-range measurements could be obtained. Romagnoli and Circi also highlighted the reduced complexity of the system, in which even adding additional satellites at the Lagrange points for redundancy would still require less than half the number of navigation satellites compared to a more traditional GNSS-like constellation in Lunar orbit. Additionally, the eight-satellite system can double as a highly-resilient communications relay with the far side of the

Moon, potentially serving as a fully redundant communications network for critical crewed missions in the future.

A similar constellation design has been proposed by Ren and Shan (2013), in which constellations were positioned across the $L_1$ and $L_2$ points. The authors investigated a number of different orbital configurations, including halo orbits, Lyapunov orbits, and Lissajous orbits. They determined a constellation of eight satellites split evenly across the northern and southern halo orbits at both $L_1$ and $L_2$ could result in a GDOP comparable to that achieved on Earth, albeit with only 50.53% of the Lunar surface receiving continuous coverage. In the conditions of Lyapunov and Lissajous orbits, the region of continuous coverage could be improved to 83.24% and 82.73% respectively, at the expense of a degraded GDOP. Ren and Shan also suggested increasing the halo orbit constellation to include six satellites in each hemisphere could maintain a similar GDOP, while improving the coverage on the Lunar surface to as much as 99.8%. Importantly, the authors noted that when these constellations were modelled with the inclusion of the Sun as a third body, the perturbations to the orbit caused additional satellites to be required to maintain the same level of performance.

### 2.3.2 Stable Triangular Points

In contrast to the relatively widely studied potential of Lunar positioning systems enabled by constellations at the colinear equilibrium points, there exists a surprising lack of significant prior research into the two stable equilibrium points, at $L_4$ and $L_5$. As seen in Figure 2.1, the triangular points are situated at a much greater distance to the Moon compared to the $L_1$ and $L_2$ points, which will result in a much greater path loss within the signal, however the geometry of the problem means augmentation satellites placed at these two locations would be approximately the same distance as the terrestrial GNSS satellites they would be augmenting.

While no artificial satellite has ever intentionally been placed at the $L_4$ or $L_5$ points long-term, the stability of these points is widely seen in nature. In the Saturnian system, there exists two pairs of so-called Trojan moons - both Tethys and Dione (discovered in 1684) each have a co-orbital Trojan moon at their respective $L_4$ and $L_5$ points, three of which were discovered in 1980, and the final as recently as 2004 (Umurhan et al. 2021). Due to the large size and mass difference between these Trojans and their co-orbital hosts, their orbits are stable as described by the CR3BP. This natural stability in an environment as complex as the Saturnian system highlights one of the potential benefits of a Lunar positioning network with nodes at these points, which would be able to be maintained in these positions for long periods with little-to-no stationkeeping requirements.

Despite being briefly mentioned by Carpenter et al. (2004) almost 20 years ago, the two stable Lagrange points have received almost no attention from researchers, potentially due to the distances involved as discussed above. The only team to have researched this in more than a passing level of detail are Zhang and Xu (2014). In this first paper, Zhang and Xu analyse different architectures of a system involving combinations of satellites at the $L_1$, $L_2$, $L_4$, and $L_5$ points, which combine to provide near-complete coverage by at least one satellite at any given time on the Lunar surface. Interestingly, they note a similar configuration of satellites at the Lagrange points of any pair of bodies could be used to improve positioning and navigation in the region, serving as ”A Universe Light House” for future missions into deep space.

Less than one year later, a follow-up article was published (Zhang and Xu 2015), investigating the navigation performance of their four-satellite constellation for a Lunar mission. In this study, it was determined that a spacecraft on a transfer trajectory from the Earth to the Moon would be in continuous coverage by at least one Lagrange satellite. In contrast to augmenting the GNSS signals, this paper discusses a method more similar to that proposed by Hill, in which direct satellite-to-satellite ranging methods are used, with measurements from all satellites com-

bined to reduce errors. While this technique does provide positioning information independent of any GNSS network, it can be modified to augment the GNSS network, improving compatibility. The same network of satellites at the Earth-Moon Lagrange points was later analysed for use on a mission to Mars, including the full trajectory from LEO to Martian orbit (Zhang and Xu 2016), suggesting potential other uses for the system beyond Lunar space. Since publication of this research, the lead author appears to have completed their PhD around 2017, and has not published any further studies in this field.

# 3 Methodology

## 3.1 GMAT Analysis

Prior to performing detailed analysis of different scenarios, a more generalised simulation was to be performed for a wider variety of scenarios. By proceeding in this way, low-resolution, short-duration simulations could be performed for many configurations, to identify candidates for further analysis. These sparse simulations were initially simulated in GMAT (General Mission Analysis Tool), and post-processed using custom Python scrips to summarise the data. Promising candidates from this stage are taken and analysed at a higher resolution, for longer periods of time, and post-processed using the same tools. For the final stage, scenario files are refined and optimised, in preparation for more detailed analysis and verification in the SkyDel GNSS simulation software.

### 3.1.1 Setup and Configuration

In order to simulate a scenario in GMAT, each satellite in the scenario must be created in the software, with parameters which define its initial conditions to propagate forward. While GMAT offers a graphical user interface for defining these, the primary method of configuring scenarios are via script files, which are plain text files used as the sole input into GMAT. The generation of these script files was automated using a Python program, in which the initial conditions of all satellites are computed and saved to the GMAT script, alongside any visualisations or outputs desired from the scenario.

To reduce computation time of these initial simulations, only a single GNSS network was included in the model, minimising the number of satellites to propagate. Data from the European Union Agency for the Space Programme (2023) regarding the the orbital parameters of the Galileo constellation were imported into Python, all back-normalised to a common reference epoch of 2016-11-21 at 00:00:00 UTC. Additionally, reference parameter rates for the orbital elements from the same source were imported, and used to propagate the orbital parameters to a start epoch of 2025-01-01 at 00:00:00 UTC. Each of these satellites had their attitude fixed to an Earth-referenced nadir pointing alignment, to allow for direction-aware visibility to be calculated in post-processing. All Galileo satellites were combined into a Formation object within GMAT, allowing them to be propagated and modelled as one, further optimising the runtime of the simulations.

A series of augmentation satellites were also added to the script, located at the $L_4$ and $L_5$ points. These two satellites were defined with a constant Moon-pointing attitude, again to enable direction-based visibility to be calculated. As the internal algorithms within GMAT define the orbits of the Earth and Moon using ephemeris files, which account for gravitational effects from a wide range of sources, it is difficult to simulate a perfect circular-restricted three body problem (CR3BP) within GMAT - this can be seen in Figure 3.1 where the location of the Moon with respect to Earth oscillates over time, causing the Lagrange points to also shift. As such, satellites placed in orbits which the CR3BP imply are stable, will gradually deviate as the deviation between the CR3BP and the true motions of the Earth and Moon grows. While this limitation meant it was not possible to model a satellite in a halo orbit around $L_2$, it did allow an approximation to be made for the $L_4$ and $L_5$ points. Over the 180-day period of the longest simulation performed, the perturbations were small enough such that placing a satellite exactly at the calculated $L_4$ and $L_5$ points resulted in them remaining near enough to the two points that analysis could be performed. The extent of this deviation can be seen in Figure 3.1 also, which highlights the inconsistency between the leading and trailing Lagrange points.

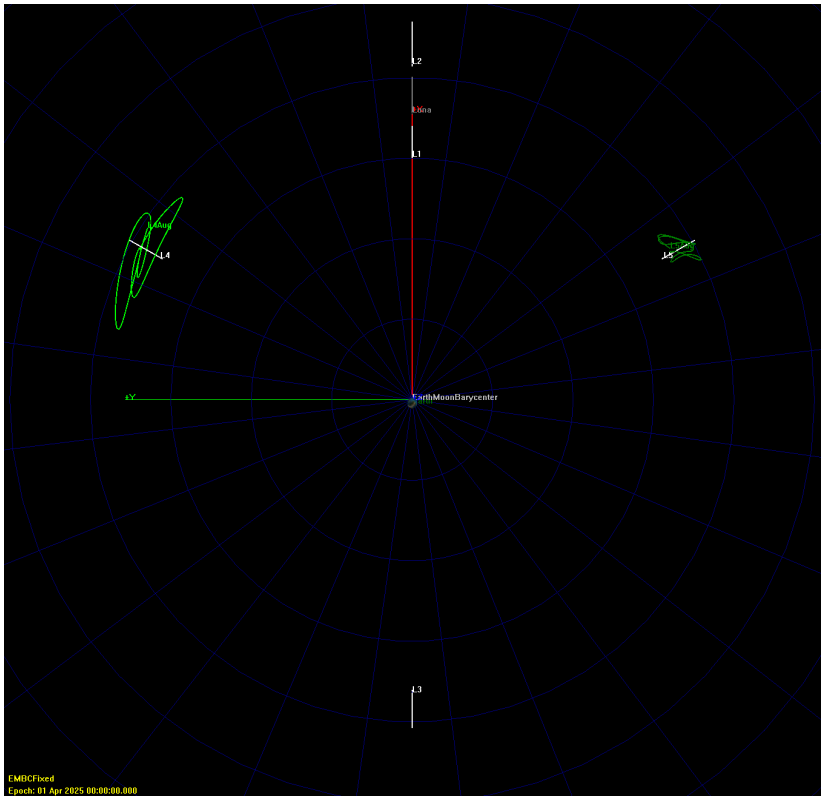


Figure 3.1: Visualisation of the rotating reference frame centred on the Earth-Moon barycentre, of a 180-day simulation in GMAT

Additional spacecraft were included in the GMAT simulation, including a range of points on the Lunar surface such as the landing sites of the six Apollo landing sites, as well as two reference spacecraft in Lunar orbit. One of which is intended to be a representative of a generic Lunar missions, modelled as a satellite travelling in a perfectly equatorial, perfectly circular orbit, with a semi-major axis of $10\,000\,\mathrm{km}$. This is intended to highlight the availability of GNSS signals on a mission which frequently passes behind the Moon, out of view of the Earth. The second reference spacecraft is intended to model the proposed Lunar Gateway, which is defined using the reference near-rectilinear halo orbit (NRHO) used by McGuire, McCarty, and Burke (2020), experiencing an average period of approximately 6.5 days. This Gateway-like reference spacecraft is intended to highlight the coverage and performance of GNSS on a critical mission, which would be a key user of GNSS in Lunar space due to the proposed operations of the space station. Both of these spacecraft were modelled in GMAT using an initial condition defined at the same starting epoch as the Galileo constellation, and were all propagated using the same time steps and force models.

### 3.1.2 Case Study Analysis

Using this input script, a 7-day GMAT simulation would be run for a range of candidate scenarios, of which the most representative would be re-simulated across a complete 180-day period. This procedure allowed for unstable configurations to be identified quickly without requiring long processing time, while allowing the most promising scenarios to be modelled to a higher level of detail using the same input configurations. From this, four case studies were modelled - of which the results are discussed in Section 4.2. These case studies included both the two reference satellites in the orbits described above, plus two surface landers - at the Apollo 11 landing site ($0.674\,16^\circ$ N, $23.473\,14^\circ$ E), and the Shackleton crater near the Lunar south pole ($89.44^\circ$ S, $38.20^\circ$ W). These surface sites were selected as representative examples of surface missions, with the Shackleton crater representing a potential landing site for the Artemis III mission (Boazman et al. 2022).

As each case study had the majority of satellites in common, the final long-duration simulation was configured such that all case studies would be simulated at the same time, and their data saved to separate locations so they can be isolated in post-processing. For each object, a number of key parameters were saved to a CSV file at each time step, which were read into a Python script in post-processing to calculate the visibility and coverage in each case study. For the Galileo and augmentation satellites, this output included the Cartesian coordinates of the satellite in an Earth-centred inertial reference frame, as well as the Euler angles representing the spacecraft's attitude. For the reference receivers in orbit, the same variables were exported, while surface-based reference receivers had attitude information omitted. In addition to all the spacecraft, the Cartesian coordinates of the Moon were also exported at each time step, to be used when calculating occlusion during post-processing. GMAT was configured to use an 8th-order Runge-Kutta orbit propagator, with a dynamic step size ranging from $1\,\mathrm{ms}$ to $45\,\mathrm{min}$ as required to model the orbits to the required level of accuracy. Further discussion about the post-processing of the case studies is discussed in Section 3.2.

### 3.1.3 Surface Coverage Mapping

In addition to modelling the four aforementioned reference receivers across a 180-day period, a modified version of the GMAT script was created to analyse the performance across the whole Lunar surface, and across Lunar orbit. This simulation involved the placement of $2700$ points evenly distributed at $5°$ spacing across the Lunar surface, at an altitude of $0\,\mathrm{km}$, $1000\,\mathrm{km}$, $5000\,\mathrm{km}$, $10\,000\,\mathrm{km}$, and $20\,000\,\mathrm{km}$. To reduce the time required to compute visibility across these 2700 points, the simulation was modified to run for a 30-day period, accounting for approximately one full orbit of the Moon around Earth. Due to limitations with the processing methods, a terrain model for the Moon was not used in this simulation, and as such the points are placed in a perfect spherical distribution along their respective altitudes above the mean surface radius. The same parameters as used in the standard simulation were exported, and processed in the same way to obtain satellite visibility, and geometric dilution of precision (GDOP).

## 3.2 Python Post-Processing

Using the data exported by GMAT, various post-processing steps were performed, to normalise the data and determine GNSS visibility and performance across the simulation. This post-processing was programmed in Python, as while many programming languages could achieve the same purpose, Python had the benefit of being simple to prototype with initially before expanding into more complex processing at a later stage. The majority of the post-processing code was developed specifically for this project, with the assistance of three third-party libraries: `numpy` (Harris et al. 2020) for data processing, `matplotlib` (Hunter 2007) for output visualisation, and `pandas` (McKinney 2010) for importing and handling of data. Each of these libraries are free and open source, and widely used within the scientific community due to their extensive capabilities.

After loading the data produced by GMAT into Python, each time step was analysed sequentially. For each step, the visibility between the receiver and every GNSS and augmentation (if applicable) satellites was calculated, using vector geometry. As GMAT was able to output the attitude of each spacecraft in terms of Euler angles, a unit vector representing the direction each satellite was pointing was able to be determined, all relative to the same Earth-centred inertial frame. Additionally, for each receiver-transmitter pair, a vector representing the path between the two satellites was calculated. Firstly, this displacement vector was used to calculate if there was an occluding body between the two satellites, by calculating if it intersected with a sphere located at the positions of the Earth or Moon. In the coordinate system used to export data, the Earth is located at the origin, and the position of the Moon is read from a file exported by GMAT.

Taking the receiver to be located at point $R$ and the transmitter at point $T$, the vector between them is represented as $\overrightarrow{RT}$. Additionally, the Moon is located at point $M$ with radius $r_M$, and the Earth at point $E$ (which is at the origin in this reference frame) with radius $r_E$. To calculate if the Moon is an occluding body, three line segments are defined creating a triangle between the three objects. These have lengths as defined below.

$$\left|\overrightarrow{RM}\right| = R - M$$
$$\left|\overrightarrow{TM}\right| = T - M$$
$$\left|\overrightarrow{RT}\right| = R - T$$

If either $\overrightarrow{RM}$ or $\overrightarrow{TM}$ have a length less than $r_M$, the two satellites will definitely be occluded by the Moon. Otherwise, if the angle between $\overrightarrow{RM}$ and $\overrightarrow{TM}$ is smaller than $90°$, then the Moon will definitely not occlude the two satellites. The angle between the two vectors can be calculated as per eq. (3.1), where $\hat{RM}$ represents the normalised unit vector of $\overrightarrow{RM}$.

$$\theta = arccos\left(\hat{RM} \cdot \hat{TM}\right) \tag{3.1}$$

If neither of these conditions are met, the minimum distance between the vector $\overrightarrow{RT}$ and the Moon $M$ must be calculated using eq. (3.2), which will be represented as $h$. If this distance is greater than $r_M$, then the two satellites are not occluded.

$$h = \overrightarrow{RM}\sqrt{1 - \left(\frac{\overrightarrow{RM} \cdot \overrightarrow{RT}}{\left|\overrightarrow{RM}\right|\left|\overrightarrow{RT}\right|}\right)^2} \tag{3.2}$$

The same process was repeated for the Earth, to determine if it is also an occluding body. Assuming neither body is occluding the view of the two satellites, their angular offset to each other is also calculated, to determine final visibility. This is to ensure GNSS satellites facing away from the Moon are not incorrectly assumed as visible. Using the same method as eq. (3.1), the angle between $\overrightarrow{RT}$ and the receiver's view vector, denoted as $\hat{R}$, is calculated. For space-based receivers, such as the Gateway-like or equatorial satellites, if this angle is less than $65°$, it is assumed the receiver is pointed such that it could receive transmissions from the GNSS satellite. This $65°$ angle was used as an approximation for receiver antenna half-beam width, based on a sample of GNSS antennas online. Alternatively, for receivers located on the Lunar surface, a maximum allowable half beam width of $90°$ was used, as it is assumed any such lander or habitation could be fitted with multiple antennae to maximise coverage. In this project, a detailed antenna gain pattern was not used, as signal strength was not a factor considered in determining the geometric distribution of GNSS signals. Additionally, the angle between $\overrightarrow{RT}$ and the transmitter's view vector, denoted as $\hat{T}$, is calculated. For this, a different allowable angular offset was allowed, which is allowed to be between $0.0°$ and $23.5°$, or between $27.0°$ $39.0°$, representing an approximation of the main and side lobes of the GNSS transmitter (Ji, Shin, and Won 2021). If mutual visibility of both satellites is achieved, and there are no occluding bodies, the transmitter in question is saved as a valid signal for that simulation step.

If in any given step, there are at least four valid visible GNSS transmitters, a calculation is made for the approximate GNSS performance. There are a number of methods for calculating this, however this project used the geometric dilution of precision, usually shortened to GDOP. The GDOP can be thought of as

the geometric quality of the signals received by a receiver, with more evenly distributed signals providing a better quality of signal than a clustered set of signals. As GDOP is used to represent the dilution of precision, it is scaled such that a perfectly distributed signal will have a GDOP of 0, and the GDOP increases as the distribution becomes less diverse. For terrestrial navigation, and GDOP of <10 is considered good, with 10-20 being recommended only for very approximate position determination. The GDOP can be calculated using the relative positions of the receiver and all signal sources.

The vector between the receiver $r$, and a GNSS satellite $i$ can be described using eq. (3.3), where $R_i$ represents the range to the satellite as given by eq. (3.4). In these equations, $x_r$, $y_r$, $z_r$ denote the absolute Cartesian position of the receiver, and $x_i$, $y_i$, $z_i$ denote the position of GNSS satellite $i$.

$$\left( \frac{x_i - x_r}{R_i}, \frac{y_i - y_r}{R_i}, \frac{z_i - z_r}{R_i} \right) \tag{3.3}$$

$$R_i = \sqrt{(x_i - x_r)^2 + (y_i - y_r)^2 + (z_i - z_r)^2} \tag{3.4}$$

For every combination of four visible satellites, a matrix $\mathbf{A}$ can be constructed, as per eq. (3.5).

$$\mathbf{A} = \begin{bmatrix} \frac{x_1 - x_r}{R_1} & \frac{y_1 - y_r}{R_1} & \frac{z_1 - z_r}{R_1} & 1 \\ \frac{x_2 - x_r}{R_2} & \frac{y_2 - y_r}{R_2} & \frac{z_2 - z_r}{R_2} & 1 \\ \frac{x_3 - x_r}{R_3} & \frac{y_3 - y_r}{R_3} & \frac{z_3 - z_r}{R_3} & 1 \\ \frac{x_4 - x_r}{R_4} & \frac{y_4 - y_r}{R_4} & \frac{z_4 - z_r}{R_4} & 1 \end{bmatrix} \tag{3.5}$$

This matrix is in turn used in the calculation of a derivative matrix, $\mathbf{Q}$, which is defined in eq. (3.6). This derived matrix can be used to find the GDOP for these four signals, as per eq. (3.7).

$$\mathbf{Q} = \left( \mathbf{A}^{\mathsf{T}} \mathbf{A} \right)^{-1} \tag{3.6}$$

$$GDOP = \sqrt{tr\left(\mathbf{Q}\right)} \tag{3.7}$$

Where more than four satellites are visible, the GDOP of all combinations is calculated, and the lowest value is used as the GDOP for that simulation step, representing the best possible geometric distribution for that instant in time. The count of visible satellites and best GDOP at each time step is exported, and saved to an output file, ready for visualisation. In the case of single-receiver case studies, this was visualised as a line plot of visibility and GDOP over time, whereas for coverage mapping simulations the whole run time output was averaged for each grid cell, and visualised in the Mollweide projection.

## 3.3 Skydel Verification

To verify the data produced by GMAT, an additional simulation was performed using the Skydel GNSS simulation software, developed by Safran. Skydel is able to simulate RF signals from a wide range of GNSS constellations, using detailed orbital data to accurately model their movement over time. It was important to perform further analysis in Skydel with additional inputs, to confirm if the analysis performed using data generated by GMAT is plausible, and to identify if the addition of other sources could benefit the performance.

Due to a number of unexpected logistical issues with regards to access to the computers with Skydel installed, as well as individual licensing issues which prevented access, the level of analysis performed in Skydel was much more limited than originally planned. Most of these issues have been resolved or mitigated against, however work continues to be done with other users within NGI who use Skydel to find a more long-term solution to some of these issues.

To minimise external effects on the simulation, a minimal GMAT script was created, to propagate the orbits of the two space-based reference receivers: a circular equatorial orbiting satellite, and a Gateway-like object in a NRHO. In contrast to the previous simulations, these were propagated with a minimum step size of $1\,\mathrm{s}$, and a maximum step size of $1\,\mathrm{h}$, over a span of 30 days, with modified settings to ensure an output which represented a suitably smooth orbit. The positions, velocities, and attitudes of the two spacecraft were exported at each time step, in a Moon-centred Moon-fixed (MCMF) coordinate reference frame, ready to be transformed in pre-processing.

### 3.3.1 Circular Restricted Three Body Problem

In order to simulate data in Skydel to the highest level of accuracy possible, the positions of the augmentation satellites were determined according to the circular restricted three body problem (CR3BP), rather than as data exported by GMAT. Within the CR3BP, the two stable Lagrange points, $L_4$ and $L_5$, have stable orbits which can be defined perfectly in the Earth-Moon plane; for the purpose of this simulation, an orbit for each in the short-period family was calculated, with a period of approximately $29.175\,\mathrm{d}$. This represents an optimal balance between closeness to the Lagrange point, and practical feasibility with respect to placing a satellite in one of these orbits. Both the short period orbits around $L_4$ and $L_5$ are perfectly stable under the approximations of the CR3BP, however interference from other sources would disturb these orbits over time in a real mission.

An additional augmentation satellite was placed at the $L_2$ point for this simulation, to examine the effects of increased coverage on the far side of the Moon, however the aforementioned limitations unfortunately prevented much analysis to be performed in this area. As the $L_2$ point, along with the rest of its colinear Lagrange points, is nominally unstable, there are no orbits which can be perfectly represented in the Earth-Moon plane. However, deviating from the plane with an initial disturbance in either the northern or southern directions can lead to an orbit known as a halo orbit, which is roughly periodic to within a degree of error. These halo orbits have a stability index greater than unity, meaning a satellite placed in such an orbit will require constant stationkeeping to maintain orbit over time. The orbit calculated for the $L_2$ augmentation satellite has a period of approximately $15.140\,\mathrm{d}$, roughly half of one Lunar orbit.

All periodic orbits in the CR3BP can be represented by a Jacobi constant, which is a dimensionless measure of the energy required to achieve this orbit. Within a family around a Lagrange point, Jacobi constants represent a unique orbit. Parameters for the three augmentation satellites can be found in Table 3.1.

Table 3.1: Reference orbital parameters for augmentation satellites

| | Family | Jacobi Constant | Period [days] | Stability Index |
|---|---|---|---|---|
| $L_2$ | Northern Halo | $3.152\,118$ | $15.139\,865$ | $606.112$ |
| $L_4$ | Short-Period | $2.987\,011$ | $29.175\,151$ | $1.000$ |
| $L_5$ | Short-Period | $2.987\,011$ | $29.175\,151$ | $1.000$ |

As all the orbits for augmentation satellites were calculated in a barycentre-centred rotating frame, they too must be transformed into a common frame prior to being used within Skydel. To reduce compounding errors during calculations, all

intermediate pre-processing of inputs prior to the simulation was performed in this rotating frame, including the orbits of the two reference receivers. This required a transformation from a MCMF reference frame, to a barycentre-centred rotating reference frame, which included translations and rotations around various axes to normalise to the same frame. The results of which can be seen in Figure 3.2, which was produced to verify the transformations were being computed correctly.

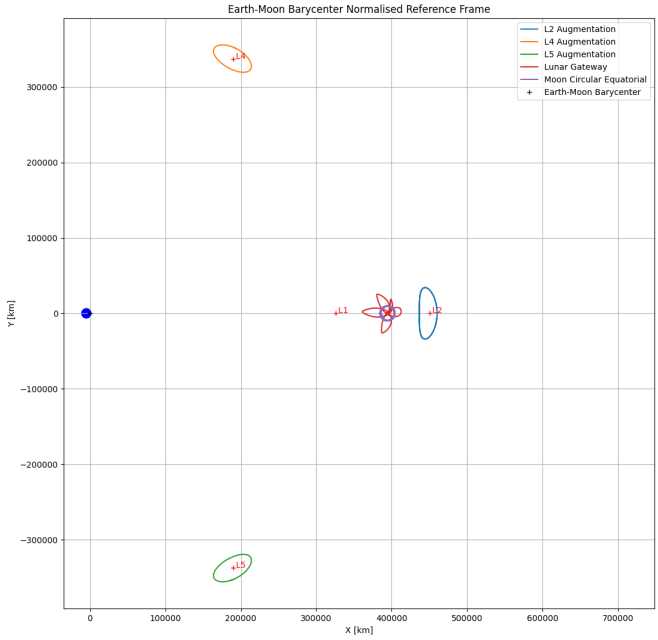


Figure 3.2: Visualisation of the positions of all GNSS augmentation satellites and reference receivers, in a barycentre-fixed rotating reference frame

Following this verification, all coordinates were transformed into an ECEF reference frame, using Cartesian coordinates, which can be recognised by Skydel. These parameters were interpolated between existing data points, to ensure a position, velocity, and angular direction (where possible) were included every 60 seconds. After exporting these ephemerides to comma-separated files, they could be imported into Skydel ready for simulation.

Skydel was configured to simulate both the Galileo and GPS constellations, in the E1 and L1 bands respectively. Augmentation satellites were modelled as an interference source, of which the position was defined using the ephemeris files generated during pre-processing. While this did not model the augmentations in exactly the same way as standard GNSS satellites with respect to the signal they produce, detailed RF and positioning data was not required from Skydel, and as such this method provided a suitable output for what was desired. The receiver was also simulated as a spacebourne receiver following a path defined by its ephermeris. For each of the two case studies, data was exported every $60\,\mathrm{s}$, despite Skydel simulating at millisecond-level precision, to reduce the data volume produced and to minimise computation time required to post-process the data. Each simulation was run for approximately the duration of one orbit of the receiver - $28\,\mathrm{h}$ for the equatorial orbiting satellite, and $200\,\mathrm{h}$ for Gateway.

The data produced by Skydel was post-processed in almost the same method described in Section 3.2. Graphical results can be seen in Chapter 4.

# 4 Results

A series of different sets of results were produced throughout the project: detailed time-series data for the four case studies presented in Section 3.1.2, coverage maps of availability in Lunar orbit and on the surface, and short-period time-series data from Skydel with the addition of GPS and an $L_2$ augmentation satellite. This chapter will present each of the different sets of results, while highlighting key points of interest, before discussing the findings and their implications in more detail in Chapter 5.

## 4.1 Data Quality

The quality of data produced was sufficient for the purposed of this research project, however higher-resolution data may have allowed finer details to be observed within the results. The split between resolution and quality was chosen to carefully balance output quality, with computation time, to avoid excessively long processing of data which would have limited the scope of the project.

Post-processing of the data took considerably longer than initially estimated, due to the large number of individual data points produced, all of which required non-trivial mathematical operations to determine their performance. As such, at some key stages during the methodology, decisions were made to limit the potential quality of output data, to ensure all data could be computed within the timeframe of the project. A key example of this is during the Skydel simulations, which produced $220\,\mathrm{MB}$ of data in a single simulation run at $60\,\mathrm{s}$ resolution, rather than the millisecond-scale Skydel is possible of. Processing of data for this simulation alone took an estimated $18\,\mathrm{h}$ of continuous compute time, greatly limiting opportunities for more detailed data in the current simulation methods.

Despite this, the data produced provides more than sufficient detail to observe key features in the results, from the signal degradation in Figure 4.1, to the outages seen in Figure 4.4, to the regions of poor visibility clearly visible in Figure 4.10. While finer resolution data may have highlighted these effects more cleanly, these important findings remain apparent in the data at present, proving the quality of data is appropriate for the scope of this project.

## 4.2 Case Studies

For each of the four case studies outlined in Section 3.1.2, the time-series results for satellite visibility, and geometric dilution of precision were calculated, which are showcased below. In order, these case studies represent: a near-rectilinear halo orbit (NRHO) modelled on a proposed orbit for the Lunar Gateway, to represent a complex mission with a particularly important demand for highly-accurate autonomous positioning; a satellite in a low-altitude circular equatorial orbit around the Moon, to represent a generic mission in which the spacecraft frequently passed behind the Moon from the perspective of Earth; the Apollo 11 landing site, to represent a surface mission with clear visibility of Earth at all times; and the Shackleton crater, to represent the location of a proposed crewed landing in the coming years. A summary of key statistics from across all four case studies can be seen in Table 4.1.

Table 4.1: Summary of results across case studies simulated

| | Augmentation Satellites | GDOP Min. | GDOP Mean | GDOP Max. | Average Visibility | 4+ Satellite Availability |
|---|---|---|---|---|---|---|
| Gateway | None | $1.15 \times 10^3$ | $2.55 \times 10^4$ | $7.17 \times 10^6$ | 2.36 | 11.92% |
| | $L_4$ + $L_5$ | $1.43 \times 10^1$ | $1.51 \times 10^2$ | $2.38 \times 10^5$ | 4.11 | 72.42% |
| Equatorial | None | $1.50 \times 10^3$ | $3.09 \times 10^4$ | $2.76 \times 10^7$ | 2.72 | 12.57% |
| | $L_4$ + $L_5$ | $1.44 \times 10^1$ | $2.37 \times 10^2$ | $6.26 \times 10^5$ | 4.22 | 74.50% |
| Apollo 11 | None | $1.48 \times 10^3$ | $1.97 \times 10^4$ | $4.57 \times 10^6$ | 2.30 | 12.71% |
| | $L_4$ + $L_5$ | $1.47 \times 10^1$ | $9.91 \times 10^1$ | $6.49 \times 10^4$ | 4.30 | 77.04% |
| Shackleton | None | $1.49 \times 10^3$ | $1.63 \times 10^4$ | $2.36 \times 10^6$ | 1.14 | 6.28% |
| | $L_4$ + $L_5$ | $1.55 \times 10^1$ | $2.95 \times 10^2$ | $5.87 \times 10^5$ | 2.16 | 27.16% |

### 4.2.1 Gateway-like NRHO

Lunar Gateway is a proposed space station in Lunar orbit, with a non-permanent crewed presence intended to support surface missions during the Artemis programme. Its orbit ranges from a low altitude over the Lunar north pole, to a very high altitude over its south pole, all while maintaining near-constant communications with Earth. As a planned hub for both crewed and robotic missions, autonomous positioning and navigation of spacecraft in the vicinity of Gateway is paramount, especially considering the round-trip communications delay between the Earth and the Moon being unsuitable for manual remote control.

As seen in Figure 4.1a, the orbit of Gateway results in periods where insufficient GNSS satellites are visible, which would severely limit logistical operations of Gateway if days-long outages in PNT were common. Even when coverage is available, the best possible GDOP experienced was in the order of $10^3$ - multiple orders of magnitude beyond what is considered acceptable for positioning on Earth.

On the other hand, when augmented with two satellites at the stable Lagrange points, $L_4$ and $L_5$, GNSS coverage becomes almost continuous, with a minimum of four satellites visible increasing from 11.92% to 72.42% of the time, greatly improving availability. In addition, the mean GDOP was reduced by two orders of magnitude, with the best GDOP experienced over the full simulation dropping to 14.3, which is sufficient for positioning in terrestrial applications. Importantly, there are periods of approximately one week long where the signal quality degrades significantly, as seen around the 100-day mark in Figure 4.1b. This sudden jump in performance appears to coincide with orbital effects, when visibility of the augmentation satellites is obscured by the Moon.

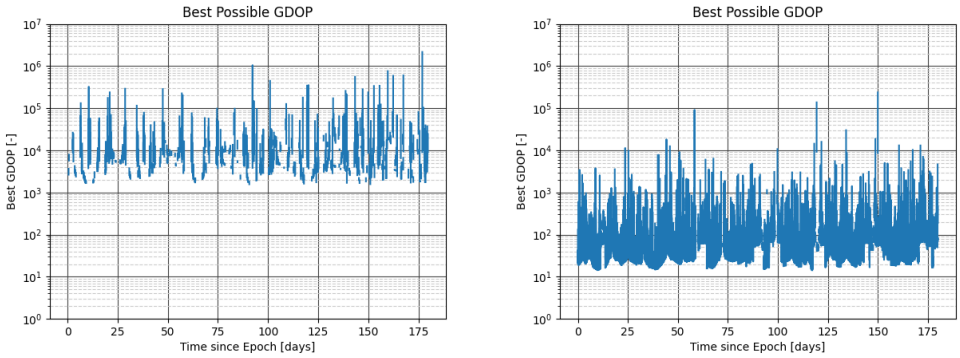


(a) Coverage from Galileo alone

(b) Galileo, augmented by $L_4$ and $L_5$

Figure 4.1: Best possible GDOP for a spacecraft in a Gateway-like NRHO, across a 180-day simulation

### 4.2.2 Low-Altitude Circular Equatorial Orbit

This case study aims to model a generic mission in Lunar orbit, in which the spacecraft frequently passes behind the moon, limiting its visibility of Earth. It was important to model this, as communications blackouts are a common occurrence in Lunar missions if communication relays are not available. As recently as August 2023, direct communication blackouts between mission controllers on ground and the Luna-25 mission delayed investigations into its propulsion anomaly, which ultimately led to it crashing on the Moon.

Similar to with Gateway, Figure 4.2a shows the GNSS network alone does not provide sufficient coverage for continuous availability, with long blackouts clearly visible in the first 50 days of the simulation. Again, the GDOP is in the order of $10^3$ at best, greatly limiting the ability to determine an accurate position from the signals available.

When compared to Figure 4.2b, the inclusion of two augmentation satellites greatly boost signal performance, raising coverage to 74.50%, with an average of 4.22 satellites visible at any given time. The effects of orbital period on the signal availability is much more pronounced in this case study, with a clear sine-like wave in the best possible GDOP, indicating the drop in signal quality when the satellite is on the opposite side of the Moon. As this satellite in particular was modelled with a semi-major axis of $10\,000\,\mathrm{km}$, complete obstruction of the terrestrial GNSS network by the Moon is rare, due to the inclination of the Moon with respect to its orbital plane.

Despite this, it is important to note the spike in GDOP at around the 175-day mark in Figure 4.2b, in which a drop in satellite visibility led to a worsening of GDOP during this period. While there are a number of potential causes for results such as these, it does highlight the importance of simulating such designs for long periods, to account for any long-period synchronicity of the orbits of the spacecraft, and the GNSS constellation.

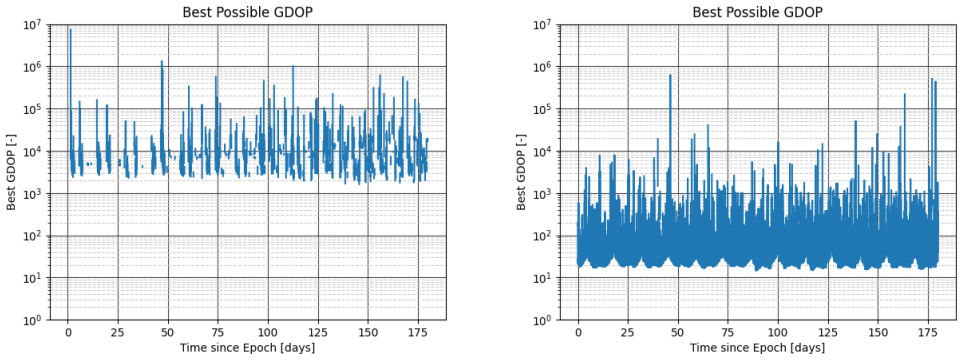


(a) Coverage from Galileo alone

(b) Galileo, augmented by $L_4$ and $L_5$

Figure 4.2: Best possible GDOP for a spacecraft in a circular equatorial Lunar orbit, across a 180-day simulation

### 4.2.3 Lunar Surface Landers

#### 4.2.3.1 Apollo 11

The landing of Apollo 11 on the Moon in 1969 was the first time humanity walked on a body other than Earth, and over 50 years later the Artemis programme is aiming to return humans to the Moon within the next decade. Selection of a landing site on the Moon is a significant decision, with a balance between technical ability, and scientific benefit. Apollo 11 landed close to the equator, and only around $23°$ east of the meridian, in an area which is continually facing the Earth. For the first crewed landing on the Moon, this central location provided the benefit of be-

ing in constant communications coverage with Earth - a feature which remains important to this day.

Despite this receiver being in continuous view of the Earth, Figure 4.3a shows GNSS signal availability is far from continuous, with long periods of blackout present due to the gradual rotation of the orbital planes of the Galileo constellation causing different groups of satellites to be in view at different times of the year.

As with the equatorial orbiting satellite, this significantly improves with the use of two augmentation satellites, especially so as both the $L_4$ and $L_5$ points have the potential to be visible from this region of the Moon. When compared to the previous case study, Figure 4.3b shows a similar minimum GDOP over time, but with a smoother maximum, indicating less fluctuation in signal quality when compared with an orbiting spacecraft. Of the four case studies simulated, the Apollo 11 landing site resulted in the highest coverage of four or more satellites, at 77.4%, with an average of 4.30 satellites visible at any time.

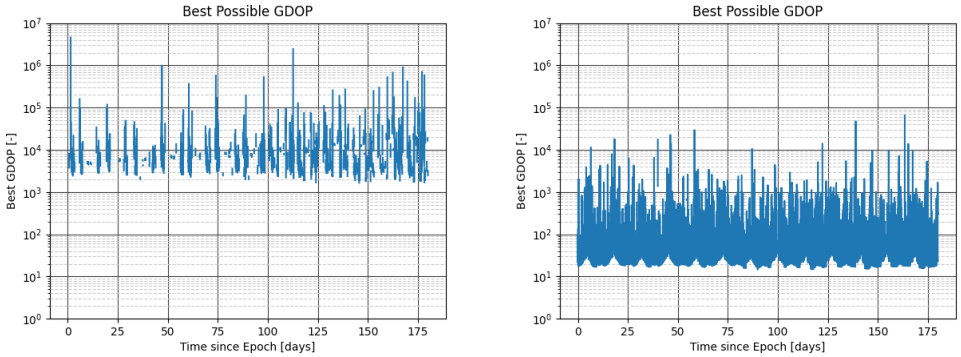


(a) Coverage from Galileo alone

(b) Galileo, augmented by $L_4$ and $L_5$

Figure 4.3: Best possible GDOP for a static surface vehicle at the Apollo 11 landing site, across a 180-day simulation

#### 4.2.3.2 Shackleton Crater

While previous crewed landings on the Moon were all within $26°$ of the equator, present and future missions to the Lunar surface land at much more extreme locations, which puts additional demands on their supporting infrastructure. With India being the first to land a craft in the region of the Moon's south pole in August 2023, and NASA targeting a polar landing site for Artemis III, the Shackleton crater case study represents one of these proposed extreme points. Studies have suggested areas of "eternal sunshine" exist around Shackleton, with near-constant illumination by the Sun making them a prime location for a solar-powered crewed base, with areas of "eternal darkness" inside the crater likely supporting large deposits of water ice.

Due to its extreme location, visibility of terrestrial satellites such as those on Earth is extremely limited, especially when considering these signals will all originate near the horizon. Figure 4.4a shows these large month-long gaps in coverage clearly, with the minimum required four satellites only visible 6.28% of the time. While missions to this location could be scheduled such that they align with the periods of good coverage, planning a mission in this way is risky, especially if delays occur mid-flight.

While this signal blackout is not avoided by the presence of $L_4$ and $L_5$ augmentation satellites, the blackouts themselves are much more regular, with periods of coverage being much more stable. This can be seen in Figure 4.4b, where the periods of coverage are continuous, and with a much improved GDOP for the central part. It can also be seen the best GDOP during these periods takes the shape

of a T, with the start and end of a coverage period experiencing a lower GDOP than the centre, due to only one of the two augmentation satellites being visible. When the visibility of both $L_4$ and $L_5$ overlap in the middle, a GDOP in the order of $10^1$ was achieved.

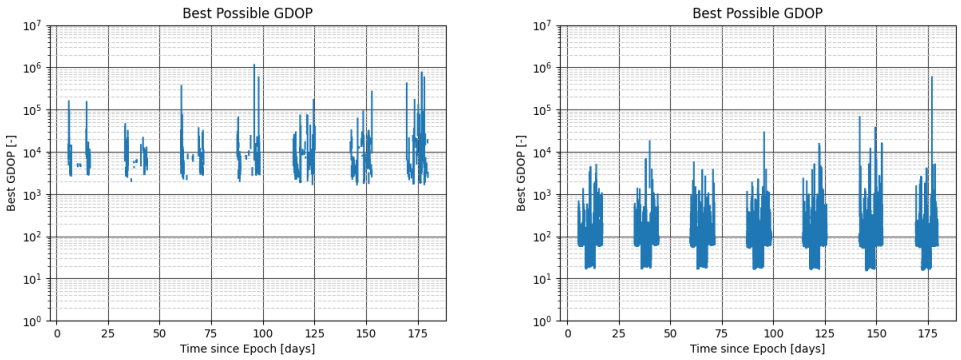


(a) Coverage from Galileo alone

(b) Galileo, augmented by $L_4$ and $L_5$

Figure 4.4: Best possible GDOP for a static surface vehicle at the Shackleton crater near the Lunar south pole, across a 180-day simulation

## 4.3 Coverage Maps

As described in Section 3.1.3, a modified simulation was developed to determine the coverage and performance across the whole Lunar surface, and shells of orbits at fixed altitudes above it. While these do not show change in coverage over time, they do present important results regarding the general availability of GNSS in Lunar space, and highlight problematic regions in which further study is required. As previously mentioned, these simulations were run across a 30 day period, and average values across this time taken and plotted.

Across the Lunar surface, visibility of the Galileo constellation is poor, with the near-side of the Moon being the only location in which a small handful of satellites are visible at any given time. As Figure 4.5 shows, this poor coverage indicates there are no regions on the Moon in which a GNSS fix can be obtained greater than 50% of the time. However, it is important to note this poor coverage is only an average, with the minimum required four satellites visible at least once during the simulation for all points on the near side of the Moon. Computing the best GDOP at all these points results in a consistent level of performance across the near-side of the Moon, although remaining well above the maximum recommended GDOP for positioning on Earth, as shown in Figure 4.6. While missions are planned to test the GNSS performance in these regions, these results suggest relying on it for safety-critical applications may be unwise.

However, the addition of two augmentation satellites at $L_4$ and $L_5$ significantly improves the average coverage of GNSS satellites, with the entire region between $30°$ E and $30°$ W of the meridian experiencing an average of greater than four visible satellites at any given time. Importantly, this region covers all landing sites from the Apollo programme, and the majority of robotic missions to the surface to date. When mapping GDOP instead of visible satellites, it can be seen this central region generally experiences an average GDOP in the order of $10^2$, which while not ideal, may be sufficient for positioning of a stationary object over time.

Two bands of poorer GDOP can be seen at approximately $20°$ north and south of the equator, as well as an arc of poorer visibility on the western side of the meridian. These artefacts are the results of orbital geometries, which over the short simulation period result in some regions of the Moon not being able to see certain plains of the Galileo constellation.

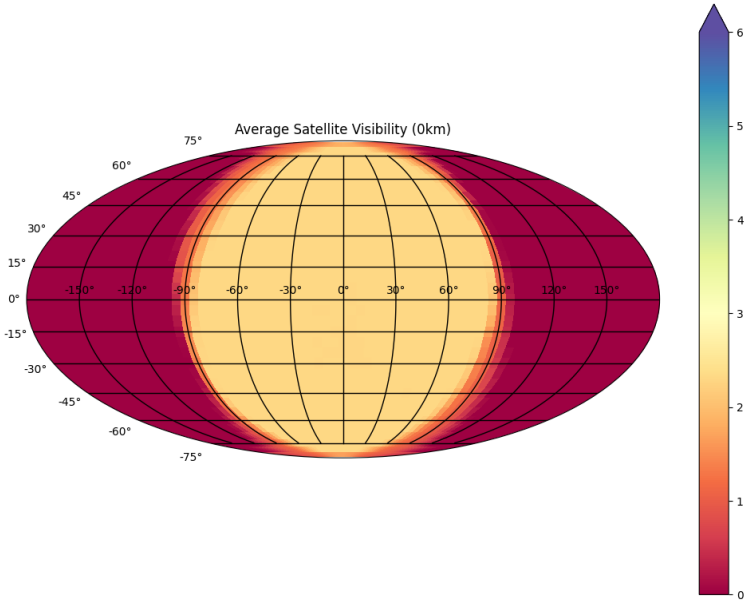


Figure 4.5: Average number of satellites visible at $5^\circ$ intervals with no augmentation satellites, across the Lunar surface (altitude = $0\,\mathrm{km}$)

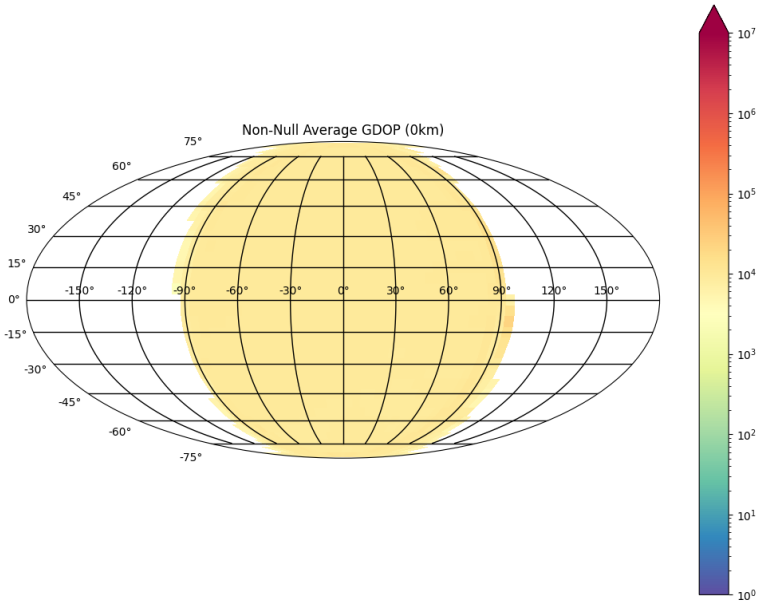


Figure 4.6: Average GDOP achieved at $5^\circ$ intervals with no augmentation satellites, across the Lunar surface (altitude = $0\,\mathrm{km}$)

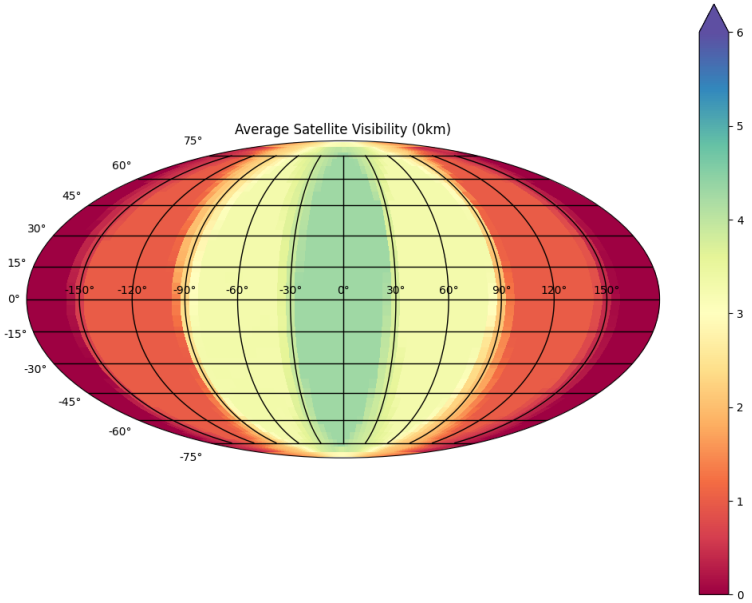


Figure 4.7: Average number of satellites visible at $5^\circ$ intervals with augmentation satellites at $L_4$ and $L_5$, across the Lunar surface (altitude = $0\,\mathrm{km}$)

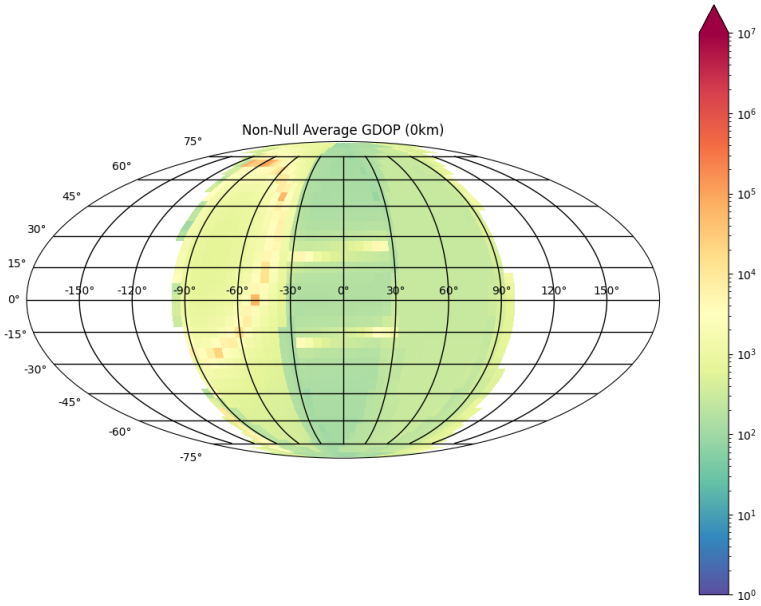


Figure 4.8: Average GDOP achieved at $5^\circ$ intervals with augmentation satellites at $L_4$ and $L_5$, across the Lunar surface (altitude = $0\,\mathrm{km}$)

As the altitude increases and a spacecraft moves further from the Lunar surface, eclipses by the Moon occur less and less frequently, resulting in greater coverage in higher orbits. This can be clearly seen in Figure 4.9, which shows the visibility of GNSS satellites at $5000\,\mathrm{km}$ above the Lunar surface is much more widespread than it was in Figure 4.5, albeit with no significant improvement in average visibility in those regions which are covered. The two red zones towards the rear of the Moon represent the small section of the orbit in which the Galileo constellation is being completely eclipsed by the Moon - a region which is only present near the equator on the far side of the Moon.

When including augmentation satellites at $L_4$ and $L_5$, the average visibility across the surface, including this eclipsed region, improves as expected, however two new regions emerge centred around $120°$ east and west of the meridian, as seen in Figure 4.10. While these may seem unusual, they represent the regions in which only one augmentation satellite is visible, with the other occluded by the Moon from the satellite's perspective. This effect is difficult to observe at lower altitudes due to the shadow of the Moon approaching this region, and less pronounced at higher altitudes due to eclipses from the Moon representing shorter and less frequent periods.

Despite these regions of reduced visibility, the presence of even a single augmentation satellite in these zones is beneficial for the GNSS receiver on board the satellite. As shown in Figure 4.11, the average GDOP across almost all $5000\,\mathrm{km}$ orbits around the Moon is in the order of $10^2$ or better, suggesting autonomous positioning of a spacecraft in this region may be possible. Plotting the same projection for minimum GDOP experienced rather than average (not shown for brevity), shows a minimum GDOP in the order of $10^1$ across the whole region, with the exception of the eclipsed regions at the very rear of the Moon.

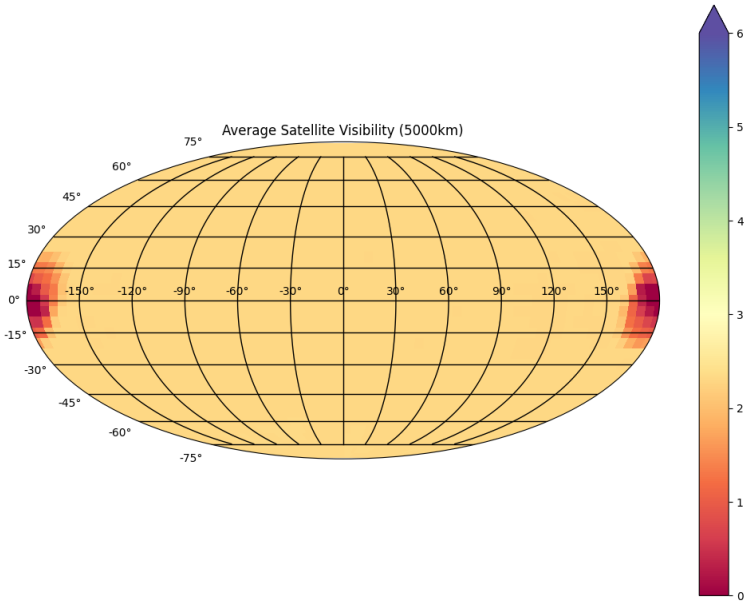


Figure 4.9: Average number of satellites visible at $5°$ intervals with no augmentation satellites, in a medium Lunar orbit (altitude = $5000\,\mathrm{km}$)

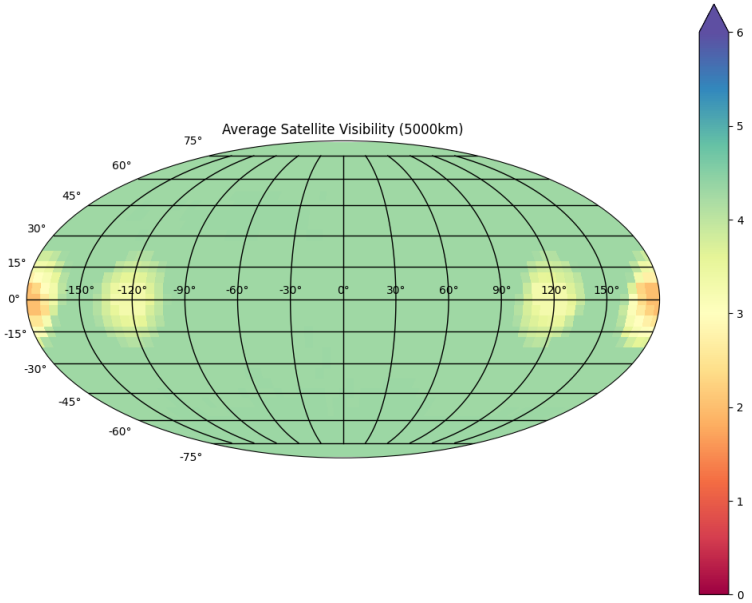


Figure 4.10: Average number of satellites visible at $5^\circ$ intervals with augmentation satellites at $L_4$ and $L_5$, in a medium Lunar orbit (altitude = $5000\,\mathrm{km}$)

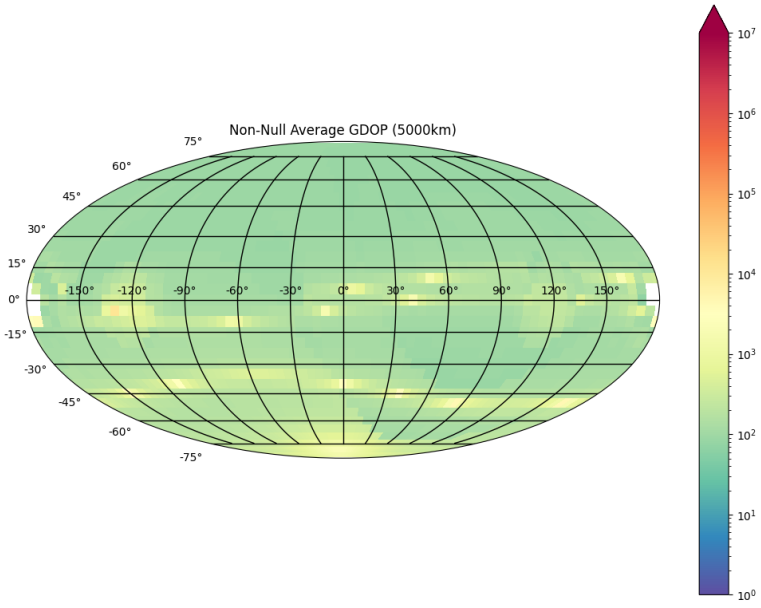


Figure 4.11: Average GDOP achieved at $5^\circ$ intervals with augmentation satellites at $L_4$ and $L_5$, in a medium Lunar orbit (altitude = $5000\,\mathrm{km}$)

Additional coverage maps for all simulations can be found in Appendix A.

## 4.4 Skydel Analysis

While time and logistical issues prevented Skydel from being used as extensively as originally planned in this research project, it was used to re-create the simulations of space-based receivers in two of the case studies: the equatorial orbiting satellite, and the Lunar Gateway. For these simulations, both the Galileo and GPS constellations were active, and an additional augmentation satellite in a halo orbit around the $L_2$ point was added to improve coverage on the far side of the Moon, where terrestrial GNSS signals would be unavailable. Both simulations were allowed to run long enough to cover one full orbit of the reference receiver with some overlap - $28\,\mathrm{h}$ for the equatorial satellite, and $200\,\mathrm{h}$ for Gateway.

### 4.4.1 Circular Equatorial Satellite

As seen in Figure 4.12, while the number of visible Galileo and GPS satellites fluctuated over the span of the simulation, the three augmentation satellites remained in near-constant view, providing an important "baseline" signal. This continuous availability of three GNSS signals from sources evenly distributed by their geometry plays a critical role in improving the performance of GNSS in Lunar space, as it reduces the reliance on the terrestrial GNSS network to provide the majority of the positioning signals, and maximises the geometric distribution of signals at all times. While pseudorange measurements from the augmentation satellites may have a greater error than the terrestrial networks due to errors in orbital determination of the augmentation satellites, their presence ensures a wide range of geometrical distribution in signals is present, and can be used to reduce errors induced by the geometry of the Earth-based GNSS signals.

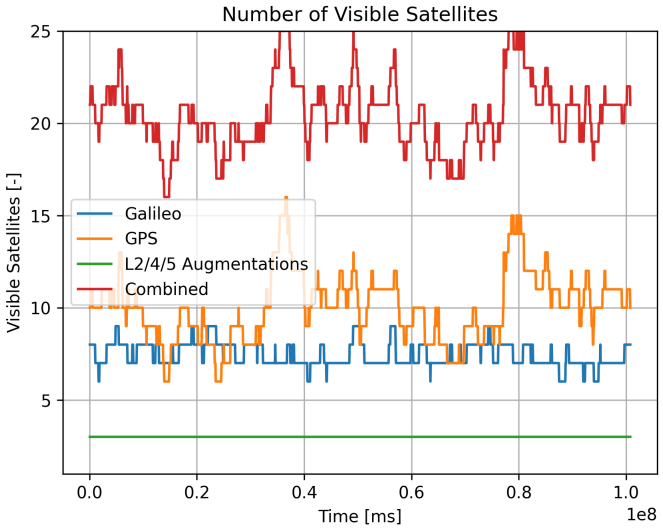


Figure 4.12: Visibility of different GNSS constellations for a circular equatorial orbiting satellite

By being able to receive signals from these three augmentation satellites, the geometric dilution of precision is vastly improved for a spacecraft in an orbit similar to the one used in this simulation, with Figure 4.13 showing a clear improvement of two orders of magnitude. Importantly, this time-series data shows the improvements to performance are consistent over the span of an orbit, with changes in visibility of the terrestrial network having minimal effect on the overall performance.

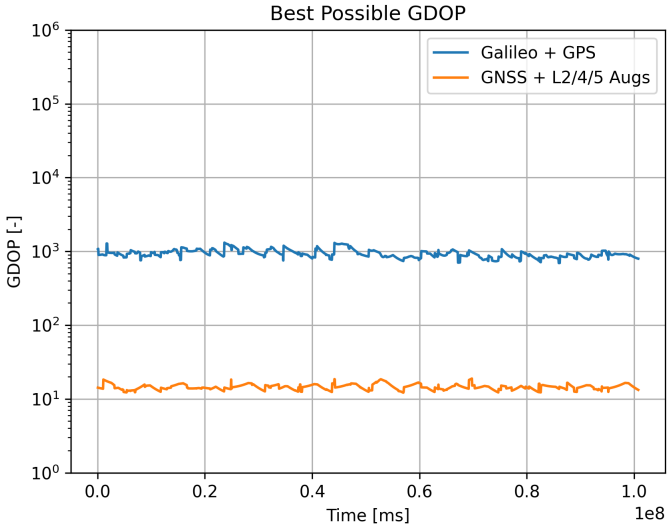


Figure 4.13: Best possible GDOP for a circular equatorial orbiting satellite, with and without augmentation satellites

### 4.4.2 Gateway-like NRHO

For a satellite in a Gateway-like NRHO, the effects of GNSS constellation patterns can be seen due to the roughly week-long orbital period. This is especially visible in the visibility of the Galileo constellation, which in Figure 4.14 can be seen to drop to as low as three near the halfway point in the simulation, and with the GPS constellation fluctuating by as much as five satellites over very short period of time. Compared to the equatorial satellite, this fluctuation in satellite visibility is much more pronounced, which not only limits the performance of a GNSS receiver, but also adds additional stress to the receiver itself, as the satellites used to produce a PNT solution will be frequently changing. However again, the use of augmentation satellites at the $L_2$, $L_4$, and $L_5$ points here have introduced a base three signals which are continually available to a receiver on Gateway, providing an important layer of stability and consistency in the signals it receives.

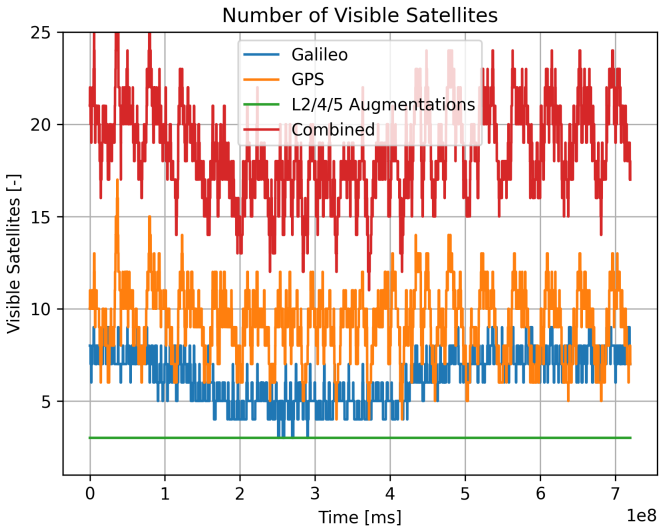


Figure 4.14: Visibility of different GNSS constellations for a Gateway-like orbit

The effects of fluctuating satellite visibility can be clearly seen in Figure 4.15, in which the best possible GDOP without augmentations is centred around $10^3$, however experiences a noticeable amount of noise as different satellites come in and out of view of the receiver. Compare this to the GDOP achieved when augmentation satellites are utilised, which is a much cleaner and consistent signal, again improved by two orders of magnitude. Importantly, towards the end of the simulation, the GDOP achieved with augmentation satellites fell below 10 - a level which would be considered sufficient for accurate positioning here on Earth, suggesting very good performance could be achieved in this orbit with relatively few augmentations.

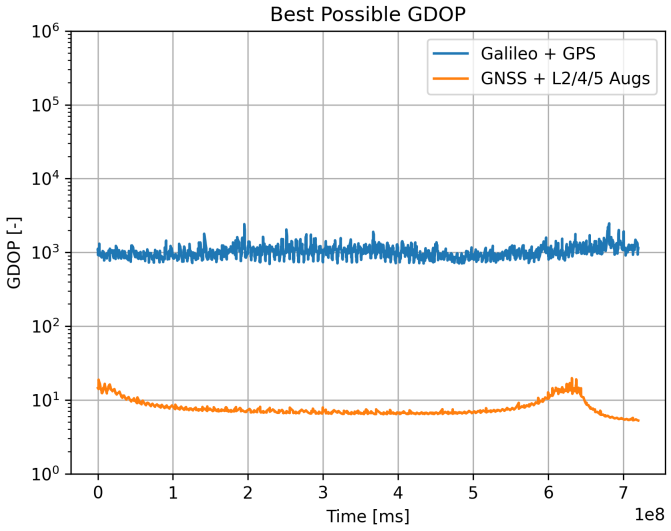


Figure 4.15: Best possible GDOP for a Gateway-like orbit, with and without augmentation satellites

# 5 Discussion

## 5.1 GNSS Performance

While an absolute measure of GNSS performance was agreed to be out of the scope of this research project, it did investigate the geometric distribution of performance by approximating GDOP. It is important to note there are a wide range of factors which can affect GNSS performance which cannot be captured by the methods used to date, such as the signal degradation due to path loss, and time dilution caused by relativity arising from the gravitational effects of the Earth and Moon. However, the geometric dilution of precision remains a key measure of performance, as a poor GDOP will greatly limit the performance, even in the absence of other disturbances.

Across all case studies presented, the geometric dilution of precision was shown to be improved by at least one order of magnitude with the inclusion of two augmentation satellites at $L_4$ and $L_5$ (Section 4.2), with a third satellite at $L_2$ further improving the GDOP to two orders of magnitude (Section 4.2), bringing it within the acceptable range for use in positioning. This improvement was consistently seen across all case studies, and was present across all regions investigated in a wide-area coverage mapping (Section 4.3). Furthermore, the use of augmentation satellites expanded the availability of GNSS signals in regions normally not serviced by terrestrial GNSS constellations, creating opportunities for navigation and positioning in regions not previously possible due to coverage limitations.

While this research project modelled the augmentation satellites in the same way as terrestrial GNSS satellites, a real-world implementation would be able to make a number of significant modifications specific to Lunar applications. GNSS satellites such as Galileo and GPS are required to provide complete coverage of the Earth from approximately $20\,000\,\mathrm{km}$ away, augmentation satellites at $L_4$ and $L_5$ would be located approximately $400\,000\,\mathrm{km}$ away from the receiver, roughly the same distance terrestrial GNSS satellites would be. However, as Lagrangian augmentation satellites may only be required to service space in proximity of the Moon, their antenna design could be modified to transmit signals that are targeted specifically at the Moon, reducing power wasted by unnecessarily transmitting signals into empty space, and allowing power to be focused on the target. Such a method could be implemented to ensure a clean, powerful signal can always be received by spacecraft in Lunar orbit, even in the absence of precise pointing. Basic trigonometry shows the full beam width of a satellite at either $L_4$ or $L_5$ could be as small as $0.489°$ to cover the full Lunar surface, which raises to $6.087°$ when covering all areas up to $20\,000\,\mathrm{km}$ in altitude. For critical missions which require precise navigation on transit to the Moon, such as crewed or robotic missions to Gateway, attitude adjustments can be made to enable the augmentation satellites to track the spacecraft across its journey, providing continuous coverage, albeit at the expense of temporarily reduced performance for spacecraft already on/near the Moon.

## 5.2 Long-Term Stability

When discussing the potential for deep space GNSS infrastructure, the long-term stability of the system is paramount, to ensure it will remain operational over the lifespan of any missions which require it. This is especially true for safety-critical missions, such as crewed flights to Gateway and the Lunar surface throughout the Artemis programme. Not only is the core infrastructure required to be redundant against outage, it must be able to achieve its objectives with minimal additional maintenance once it is operational.

The two short-period orbits described in Section 3.3.1 for the $L_4$ and $L_5$ satellites are nominally stable under the approximations of the circular restricted three

body problem, indicating in an absence of perturbations, spacecraft in these orbits will remain there in perpetuity. Unfortunately, the CR3BP is an idealised case, and does not accurately model the complex solar system, with its hundreds of bodies moving together in one dynamic system, each contributing a small disturbance to objects within. Despite this, the natural stability of the triangular Lagrange points is widespread in nature, as discussed in Section 2.3.2, with a number of moons in the Saturnian system located in stable orbits at $L_4$ and $L_5$ points of parent bodies, and countless objects captured in the Earth-Moon system near its $L_4$ and $L_5$ points. While no artificial satellite has ever intentionally been placed in an orbit around any $L_4$ or $L_5$ point, studies into the concept have shown it would be possible for such a satellite to remain in its desired orbit over a sufficiently long time span with minimal station-keeping efforts.

On the contrary, the $L_2$ point is nominally unstable, even in the absence of perturbations from other bodies, requiring station-keeping efforts at regular intervals to maintain the orbit. While this does limit the lifespan of a potential augmentation satellite at the $L_2$ point, previous missions to the Sun-Earth $L_2$ point have been designed with a lifespan in the order of 6-10 years with less than $100\,\mathrm{m}\cdot\mathrm{s}^{-1}$ $\Delta v$ in total station-keeping consumables. Through careful mission planning, it is possible to extend this lifespan without requiring additional fuel, as experienced with the James Webb Space Telescope, which is predicted to be able to remain in place for 20 years as a result of careful orbital insertion (Amos 2022).

Outside of orbital stability, long-term stability of the performance of the augmentation satellites is not expected to be a concern. As of 2023, the GPS constellation operated by the United States includes satellites launched 20 years prior, and the Galileo constellation continues to use its first batch of satellites launched in 2014. As augmentation satellites would likely be of a very similar design to terrestrial GNSS satellites by nature, the longevity of the hardware is well established, albeit not outside of medium-Earth orbit.

## 5.3 Limitations

While the results presented here show a promising potential for improving GNSS availability in Lunar space, it is important to note the limitations of their implications. The models used to simulate the scenarios presented in these results are approximations, which intentionally omit certain higher-order effects for the sake of simplicity. As such, these results represent an idealised case, in which stable orbits can be maintained, and disturbances can be negated. Despite this, the output of this research shows a strong case for exploring the use of Lagrange points for Lunar missions moving forwards, as the opportunity they present for improving GNSS performance is significant, with a much reduced system complexity compared to some of the constellations discussed in Section 2.1. As discussed further in Section 6.2, the model used to date will be improved and refined, gradually adding in additional complexities to better represent the true dynamics of a system such as this.

On the other hand, it is important to consider the limitations of the methodology used within this research. While the methodology discussed in Chapter 3 was carefully planned to maximise research output, unforeseen decisions throughout the research project led to simplifications being required, such as shortening the duration of simulations to ensure they could run in a reasonable length of time, as well as artificial resolution limits to ensure data could be processed within the time frame of the project. While this proved suitable for the project at hand, these limiting factors will need to be revised and optimised as the work continues in the future to minimise their impact.

# 6 Conclusions

## 6.1 Research Evaluation

The work presented in this dissertation showcases the untapped potential of the Lagrange points for improving GNSS performance and availability on Lunar missions. Their unique geometrical locations compared to Earth gives rise to a significant improvement in signal distribution, which combined with the pseudo-stationary effect the satellites would have from a static observer on the Moon, makes them prime for use as a continually-available augmentation signal. As discussed in the previous sections, the results produced from this research show an improvement in performance of several orders of magnitude compared to the terrestrial GNSS network alone, bringing the geometric dilution of precision down to a level suitable for autonomous positioning and navigation. The results obtained fulfil the aims and objectives set out in Chapter 1, and lay down a clear path forward for continuing to develop this research area in the coming years.

## 6.2 Future Work

Moving forwards, there are a number of key areas in which the research performed here can be improved, starting with higher-fidelity simulations of different cases. At key points throughout this project, a trade-off was made between simulation detail, and processing time, often with the latter being prioritised to maximise the number of options to be explored. From the results of this research project, the cases being investigated can be refined, and more detailed analysis of those cases can be performed. Through improvements to the efficiency of the code used for post-processing, including the introduction of multi-threaded processing where possible, it is hoped the work performed to date can lead to continued studies in a much greater depth than what has been discussed here.

Additionally, future work in this area would benefit from improvements in the modelling methods and assumptions used throughout this work. Due to the limited scope of the project, advanced orbital models beyond the circular restricted three body problem were not considered, and effects such as Solar, Jovian, and Venusian gravitational perturbations were omitted, despite their non-trivial impact on orbits in the real world. Similarly, effects such as the libration of the Moon were omitted from the model, as well as surface features which would impact visibility from certain regions on the surface. Moving forwards, it is planned each of these additional effects, among others, should be gradually implemented into the model, to ensure it is more representative of the true dynamics of the missions proposed.

Furthermore, once a stable model has been defined for the problem, including the perturbations mentioned above, it is hoped additional information regarding antenna patterns, signal distribution, and other RF factors can be included in the model. Many of these features can be achieved via the Skydel simulation package, which were not explored in this research project to avoid unnecessary complexity at this time, however are possible to model and explore the physical characteristics of GNSS signals in Lunar space. It is hoped upcoming missions to the Moon, including the LuGRE mission tentatively scheduled for launch later this year (Parker et al. 2022), will be able to provide critical *in situ* GNSS data from Lunar orbit and the surface, providing key truth data to validate these models against.

# Bibliography

Amos, Jonathan (Jan. 8, 2022). "James Webb telescope completes epic deployment sequence". In: *BBC News*. URL: https://www.bbc.co.uk/news/science-environment-59914936.

Arcia Gil, Angel David et al. (Mar. 2023). "Methodology for optimizing a Constellation of a Lunar Global Navigation System with a multi-objective optimization algorithm". In: *Acta Astronautica* 204, pp. 348–357. ISSN: 00945765. DOI: 10.1016/j.actaastro.2023.01.003.

Boazman, Sarah. J. et al. (Dec. 1, 2022). "The Distribution and Accessibility of Geologic Targets near the Lunar South Pole and Candidate Artemis Landing Sites". In: *The Planetary Science Journal* 3.12, p. 275. ISSN: 2632-3338. DOI: 10.3847/PSJ/aca590. URL: https://iopscience.iop.org/article/10.3847/PSJ/aca590.

Carpenter, J. Russell et al. (Aug. 16, 2004). "Libration Point Navigation Concepts Supporting the Vision for Space Exploration". In: *AIAA/AAS Astrodynamics Specialist Conference and Exhibit*. AIAA/AAS Astrodynamics Specialist Conference and Exhibit. Providence, Rhode Island: American Institute of Aeronautics and Astronautics. ISBN: 978-1-62410-075-8. DOI: 10.2514/6.2004-4747.

Delépaut, Anaïs, Pietro Giordano, et al. (Dec. 2020). "Use of GNSS for lunar missions and plans for lunar in-orbit development". In: *Advances in Space Research* 66.12, pp. 2739–2756. ISSN: 02731177. DOI: 10.1016/j.asr.2020.05.018. URL: https://linkinghub.elsevier.com/retrieve/pii/S0273117720303410 (visited on 08/13/2023).

Delépaut, Anaïs, Miriam Schönfeldt, et al. (Oct. 11, 2019). "A System Study for Cislunar Radio Navigation Leveraging the Use of Realistic Galileo and GPS Signals". In: 32nd International Technical Meeting of the Satellite Division of The Institute of Navigation (ION GNSS+ 2019). Miami, Florida, pp. 1199–1219. DOI: 10.33012/2019.17084.

Euler, Leonhard (1767). "De motu rectilineo trium corporum se mutuo attrahentium". In: *Novi Commentarii academiae scientiarum Petropolitanae* 11, pp. 144–151.

European Union Agency for the Space Programme (Apr. 2023). *Orbital and Technical Parameters | European GNSS Service Centre*. Orbital and Technical Parameters. URL: https://www.gsc-europa.eu/system-service-status/orbital-and-technical-parameters.

Guan, Meiqian et al. (Jan. 11, 2022). "Navigation in GEO, HEO, and Lunar Trajectory Using Multi-GNSS Sidelobe Signals". In: *Remote Sensing* 14.2, p. 318. ISSN: 2072-4292. DOI: 10.3390/rs14020318.

Harris, Charles R. et al. (Sept. 17, 2020). "Array programming with NumPy". In: *Nature* 585.7825, pp. 357–362. ISSN: 0028-0836, 1476-4687. DOI: 10.1038/s41586-020-2649-2. URL: https://www.nature.com/articles/s41586-020-2649-2.

Hill, Keric A. (2007). "Autonomous Navigation in Libration Point Orbits". Doctoral Thesis. University of Colorado. 172 pp.

Hunter, John D. (2007). "Matplotlib: A 2D Graphics Environment". In: *Computing in Science & Engineering* 9.3, pp. 90–95. ISSN: 1521-9615. DOI: 10.1109/MCSE.2007.55. URL: http://ieeexplore.ieee.org/document/4160265/.

Ji, Gun-Hoon, Ki-Ho Kwon, and Jong-Hoon Won (Sept. 26, 2021). "GNSS Signal Availability Analysis in SSV for Geostationary Satellites Utilizing multi-GNSS with First Side Lobe Signal over the Korean Region". In: *Remote Sensing* 13.19, p. 3852. ISSN: 2072-4292. DOI: 10.3390/rs13193852. URL: https://www.mdpi.com/2072-4292/13/19/3852.

Ji, Gun-Hoon, Heon Shin, and Jong-Hoon Won (2021). "Analysis of multi-constellation GNSS receiver performance utilizing 1-st side-lobe signal on the use of SSV for KPS satellites". In: *IET Radar, Sonar & Navigation* 15.5, pp. 485–499. ISSN: 1751-8792. DOI: 10.1049/rsn2.12052.

Jun, William W. et al. (Apr. 2022). "A Minimal Architecture for Real-Time Lunar Surface Positioning Using Joint Doppler and Ranging". In: *IEEE Transactions on Aerospace and Electronic Systems* 58.2, pp. 1367–1376. ISSN: 0018-9251, 1557-9603, 2371-9877. DOI: 10.1109/TAES.2021.3122876.

Konin, Valeriy and Fedir Shyshkov (Dec. 2016). "Autonomous navigation of service spacecrafts on geostationary orbit using GNSS signals". In: *Radioelectronics and Communications Systems* 59.12, pp. 562–566. ISSN: 0735-2727, 1934-8061. DOI: 10.3103/S0735272716120049. URL: http://link.springer.com/10.3103/S0735272716120049.

Lagrange, Joseph-Louis (1867). "Tome 6, Chapitre II: Essai sur le problème des trois corps". In: *Œuvres de Lagrange*. Paris: Gauthier-Villars, pp. 229–334.

McGuire, Melissa L., Steven L. McCarty, and Laura M. Burke (Mar. 1, 2020). *Power and Propulsion Element (PPE) Spacecraft Reference Trajectory Document*. GRC-E-DAA-TN72909. NTRS Author Affiliations: Glenn Research Center NTRS Document ID: 20200002143 NTRS Research Center: Glenn Research Center (GRC).

McKinney, Wes (2010). "Data Structures for Statistical Computing in Python". In: Python in Science Conference. Austin, Texas, pp. 56–61. DOI: 10.25080/Majora-92bf1922-00a. URL: https://conference.scipy.org/proceedings/scipy2010/mckinney.html.

Musumeci, Luciano et al. (June 2016). "Design of a High Sensitivity GNSS receiver for Lunar missions". In: *Advances in Space Research* 57.11, pp. 2285–2313. ISSN: 02731177. DOI: 10.1016/j.asr.2016.03.020.

Office of the United States Secretary of Commerce (May 1, 2000). *Fact Sheet: Civilian Benefits of Discontinuing Selective Availability (Press Release)*. In collab. with Morrie Goodman and Steven Jacques. URL: https://www.gps.gov/systems/gps/modernization/sa/benefits/.

Parker, Joel J.K. et al. (Feb. 14, 2022). "The Lunar GNSS Receiver Experiment (LuGRE)". In: 2022 International Technical Meeting of The Institute of Navigation. Long Beach, California, pp. 420–437. DOI: 10.33012/2022.18199.

Ren, Yuan and Jinjun Shan (Apr. 2013). "Libration point orbits for lunar global positioning systems". In: *Advances in Space Research* 51.7, pp. 1065–1079. ISSN: 02731177. DOI: 10.1016/j.asr.2012.10.022.

Romagnoli, Daniele and Christian Circi (Aug. 2010). "Lissajous trajectories for lunar global positioning and communication systems". In: *Celestial Mechanics and Dynamical Astronomy* 107.4, pp. 409–425. ISSN: 0923-2958, 1572-9478. DOI: 10.1007/s10569-010-9279-1.

Shirobokov, Maksim, Sergey Trofimov, and Mikhail Ovchinnikov (Oct. 2021). "Lunar frozen orbits for small satellite communication/navigation constellations".

In: *International Astronautical Congress*. International Astronautical Congress (IAC). Dubai, United Arab Emirates.

Trofimov, Sergey, Maksim Shirobokov, and Mikhail Ovchinnikov (Sept. 2022). "Design and Study of Satellite Constellations in Frozen Low Lunar Orbits". In: *International Astronautical Congress*. International Astronautical Congress (IAC). Paris, France.

UK Space Agency (Feb. 27, 2023). *UK companies to provide services for future Moon missions*. GOV.UK. URL: https://www.gov.uk/government/news/uk-companies-to-provide-services-for-future-moon-missions (visited on 03/22/2023).

Umurhan, Orkan M. et al. (Nov. 2021). "Modeling global-scale mass flows on the Lagrangian satellites of Dione and Tethys". In: *Icarus* 369, p. 114612. ISSN: 00191035. DOI: 10.1016/j.icarus.2021.114612. URL: https://linkinghub.elsevier.com/retrieve/pii/S0019103521002773.

Wijnen, Mick et al. (Feb. 2018). "CubeSat Lunar Positioning System Enabled by Novel On-Board Electric Propulsion". In: *IEEE Transactions on Plasma Science* 46.2, pp. 319–329. ISSN: 0093-3813, 1939-9375. DOI: 10.1109/TPS.2017.2779756.

Winternitz, Luke B. et al. (June 2017). "Global Positioning System Navigation Above 76,000 KM for NASA'S Magnetospheric Multiscale Mission". In: *NAVIGATION* 64.2, pp. 289–300. ISSN: 0028-1522, 2161-4296. DOI: 10.1002/navi.198.

Zhang, Lei and Bo Xu (Sept. 2014). "A Universe Light House — Candidate Architectures of the Libration Point Satellite Navigation System". In: *Journal of Navigation* 67.5, pp. 737–752. ISSN: 0373-4633, 1469-7785. DOI: 10.1017/S0373463314000137.

Zhang, Lei and Bo Xu (Mar. 2015). "Navigation Performance of the Libration Point Satellite Navigation System in Cislunar Space". In: *Journal of Navigation* 68.2, pp. 367–382. ISSN: 0373-4633, 1469-7785. DOI: 10.1017/S0373463314000617.

Zhang, Lei and Bo Xu (Jan. 2016). "Navigation Performance of the Libration Point Satellite Navigation System for Future Mars Exploration". In: *Journal of Navigation* 69.1, pp. 41–56. ISSN: 0373-4633, 1469-7785. DOI: 10.1017/S0373463315000478.

# A Additional Coverage Maps

As described in Section 3.1.3, a number of coverage maps of GNSS visibility and performance were produced. While only a select few of these were discussed in Section 4.3, the remainder are shown in this appendix, for further reading. All maps are shown in the Mollweide projection, with the same colour scale, for easy comparison between different simulations.

## Lunar Surface ($0\,\mathrm{km}$ altitude)

### Average Satellite Visibility

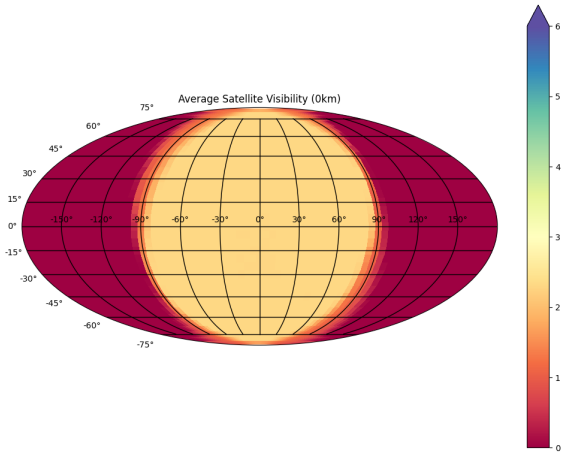


Figure A.1: Average number of satellites visible at $5°$ intervals with no augmentation satellites, across the Lunar surface (altitude = $0\,\mathrm{km}$)

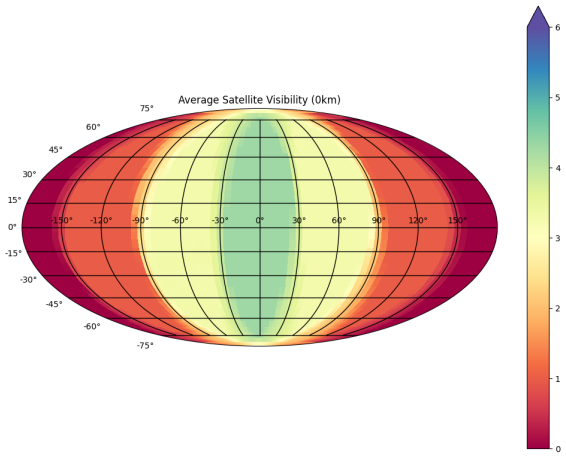


Figure A.2: Average number of satellites visible at $5°$ intervals with augmentation satellites at $L_4$ and $L_5$, across the Lunar surface (altitude = $0\,\mathrm{km}$)

## Average GDOP

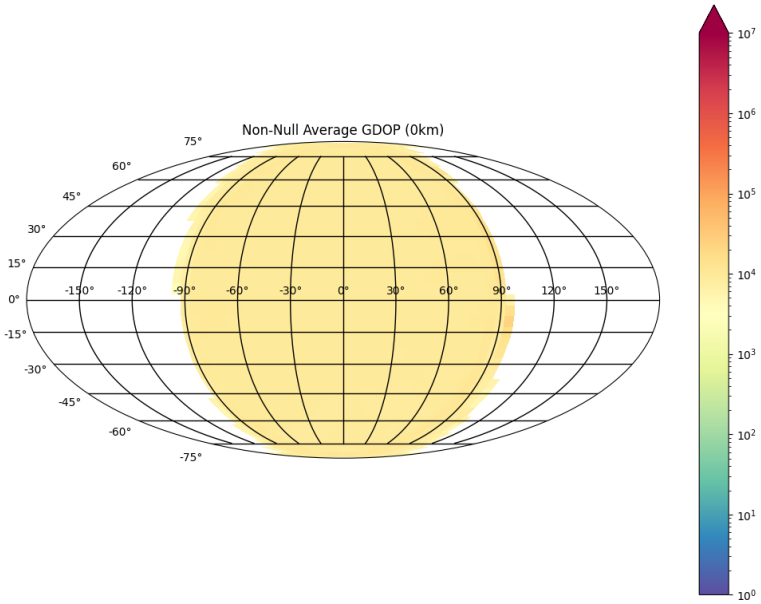


Figure A.3: Average GDOP across $5°$ intervals with no augmentation satellites, across the Lunar surface (altitude = $0\,\mathrm{km}$)

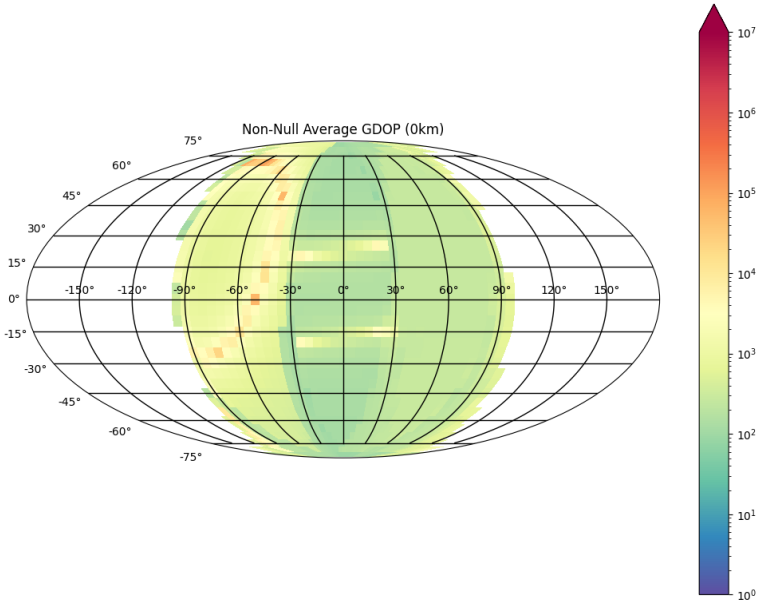


Figure A.4: Average GDOP across $5°$ intervals with augmentation satellites at $L_4$ and $L_5$, across the Lunar surface (altitude = $0\,\mathrm{km}$)

## Low Lunar Orbit ($1000\,\mathrm{km}$ altitude)
### Average Satellite Visibility

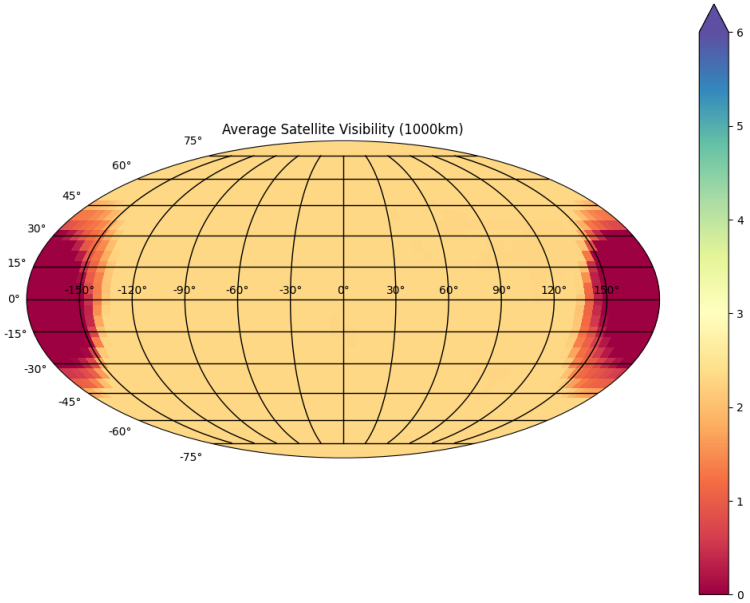


Figure A.5: Average number of satellites visible at $5°$ intervals with no augmentation satellites, in a low Lunar orbit (altitude = $1000\,\mathrm{km}$)

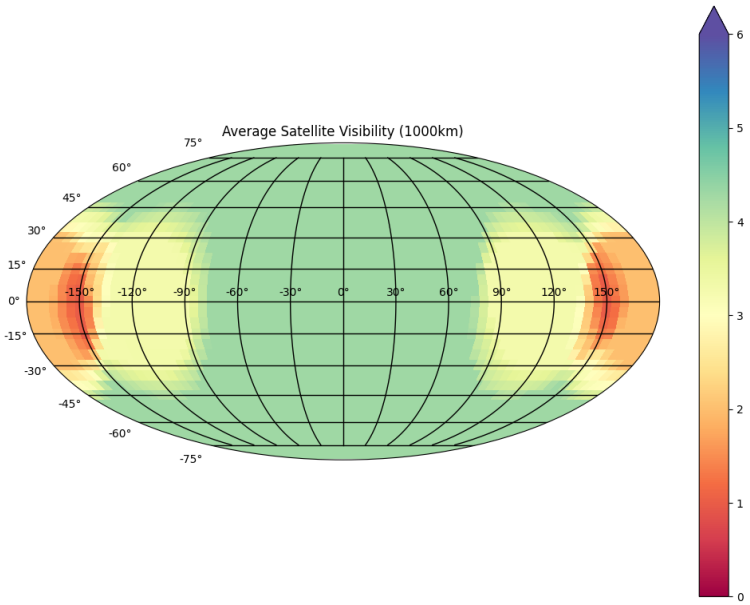


Figure A.6: Average number of satellites visible at $5°$ intervals with augmentation satellites at $L_4$ and $L_5$, in a low Lunar orbit (altitude = $1000\,\mathrm{km}$)

## Average GDOP

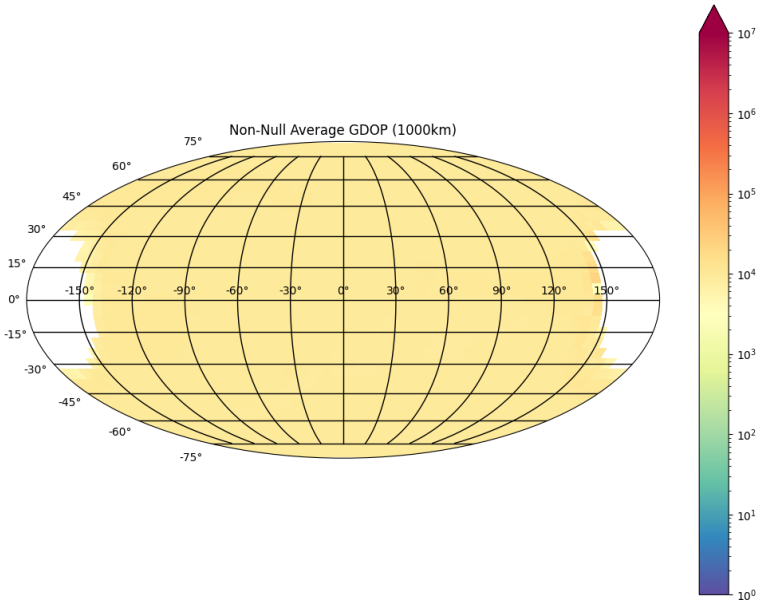


Figure A.7: Average GDOP across $5°$ intervals with no augmentation satellites, in a low Lunar orbit (altitude = $1000\,\mathrm{km}$)

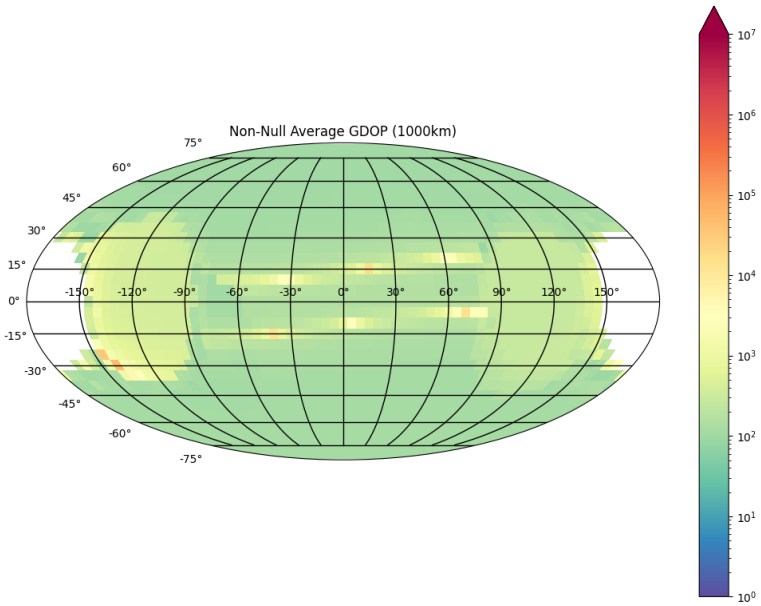


Figure A.8: Average GDOP across $5°$ intervals with augmentation satellites at $L_4$ and $L_5$, in a low Lunar orbit (altitude = $1000\,\mathrm{km}$)

## Medium Lunar Orbit ($5000\,\mathrm{km}$ altitude)

### Average Satellite Visibility

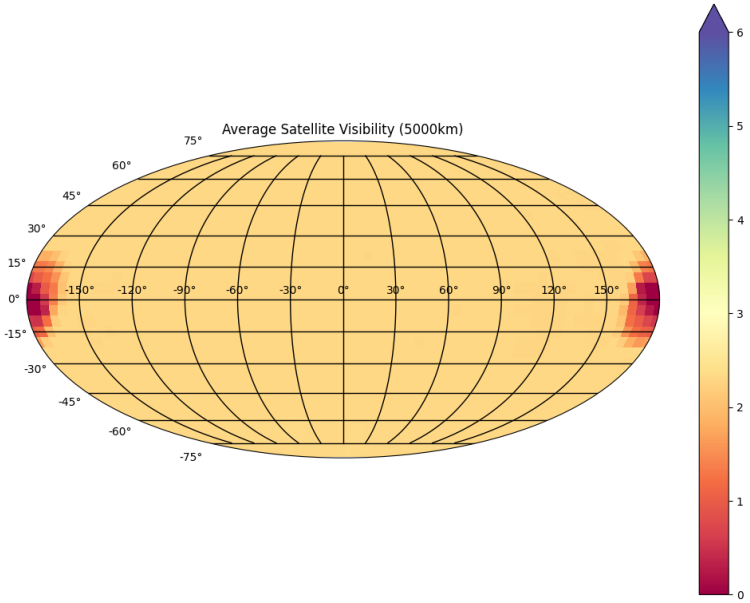


Figure A.9: Average number of satellites visible at $5°$ intervals with no augmentation satellites, in a medium Lunar orbit (altitude = $5000\,\mathrm{km}$)

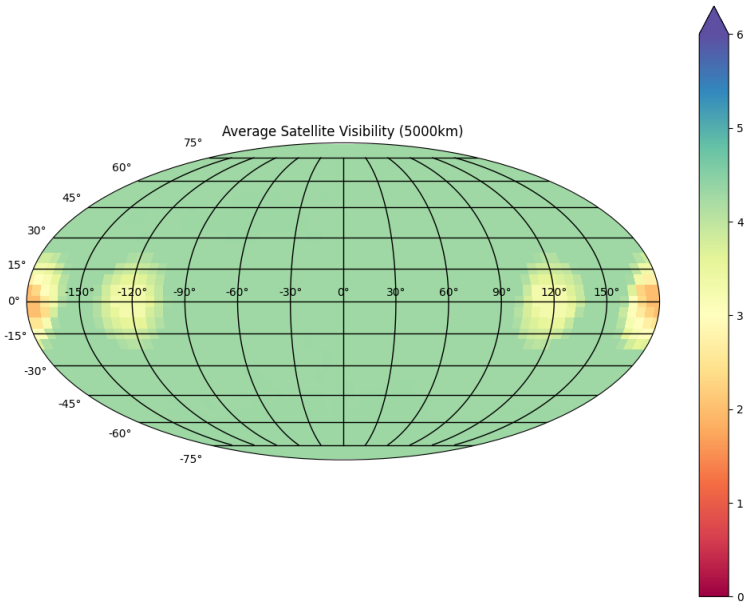


Figure A.10: Average number of satellites visible at $5°$ intervals with augmentation satellites at $L_4$ and $L_5$, in a medium Lunar orbit (altitude = $5000\,\mathrm{km}$)

## Average GDOP

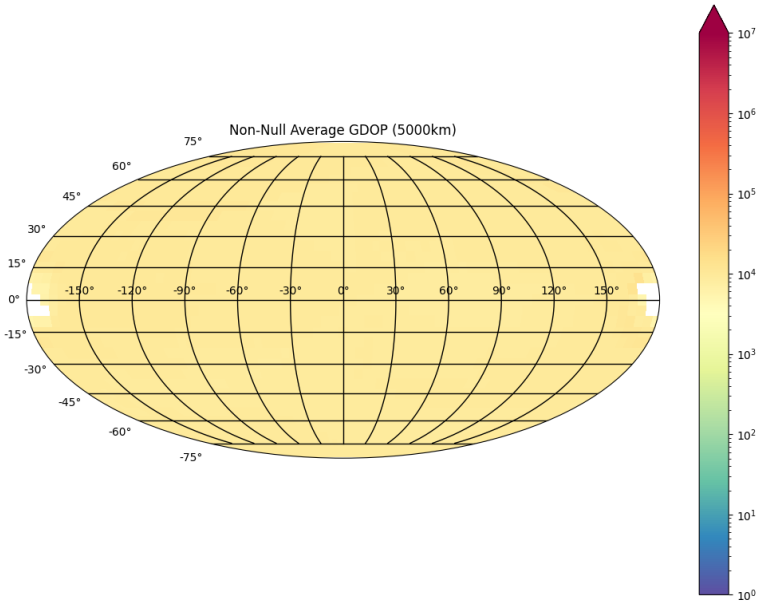


Figure A.11: Average GDOP across $5°$ intervals with no augmentation satellites, in a medium Lunar orbit (altitude = $5000\,\mathrm{km}$)

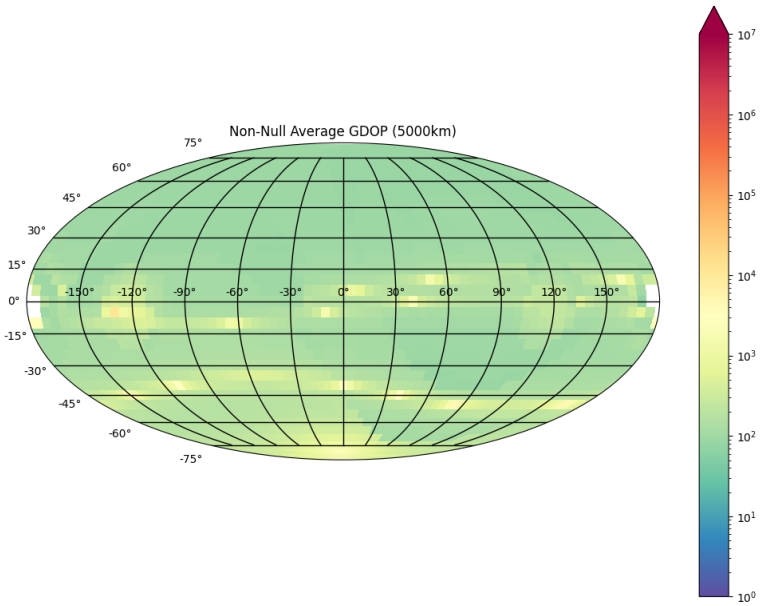


Figure A.12: Average GDOP across $5°$ intervals with augmentation satellites at $L_4$ and $L_5$, in a medium Lunar orbit (altitude = $5000\,\mathrm{km}$)

## High Lunar Orbit ($10\,000\,\mathrm{km}$ altitude)
### Average Satellite Visibility

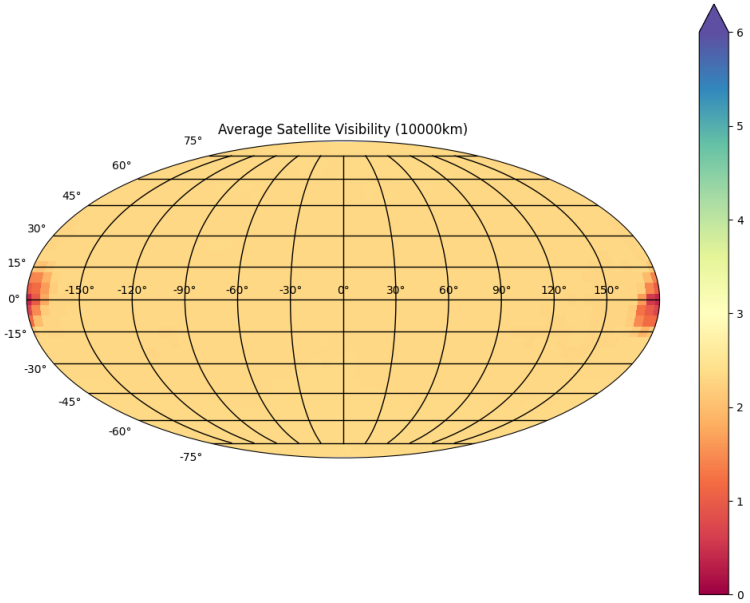


Figure A.13: Average number of satellites visible at $5°$ intervals with no augmentation satellites, in a high Lunar orbit (altitude = $10\,000\,\mathrm{km}$)

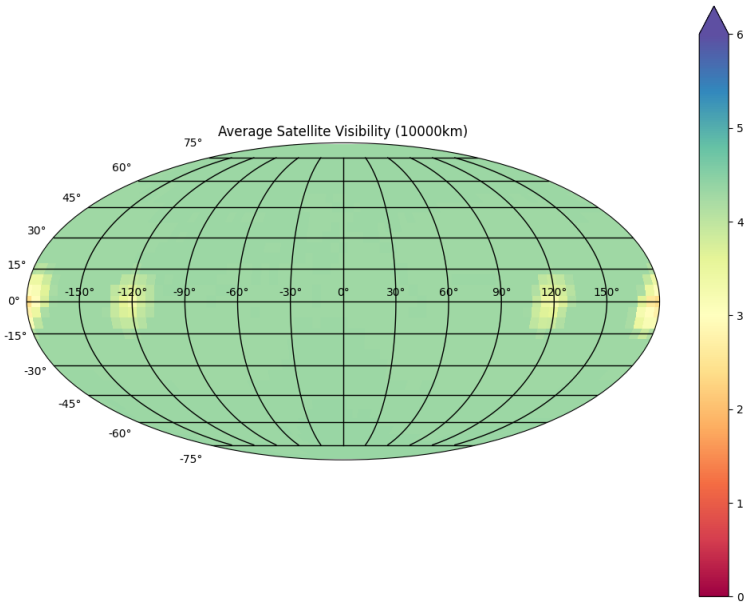


Figure A.14: Average number of satellites visible at $5°$ intervals with augmentation satellites at $L_4$ and $L_5$, in a high Lunar orbit (altitude = $10\,000\,\mathrm{km}$)

## Average GDOP

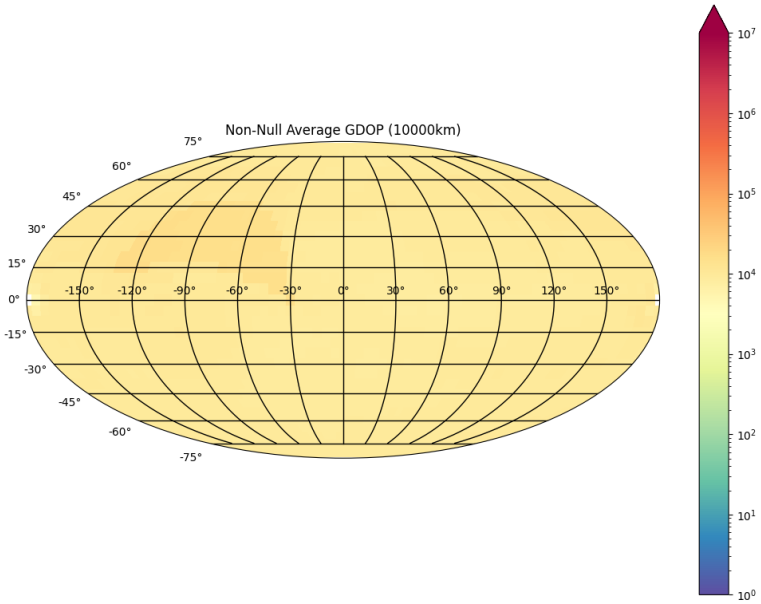


Figure A.15: Average GDOP across $5°$ intervals with no augmentation satellites, in a high Lunar orbit (altitude = $10\,000\,\mathrm{km}$)

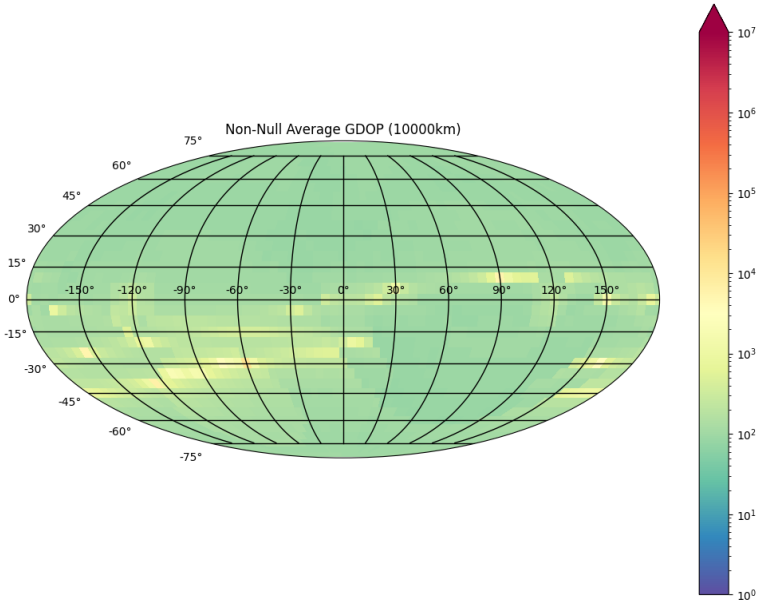


Figure A.16: Average GDOP across $5°$ intervals with augmentation satellites at $L_4$ and $L_5$, in a high Lunar orbit (altitude = $10\,000\,\mathrm{km}$)

# Very High Lunar Orbit ($20\,000\,\mathrm{km}$ altitude)

## Average Satellite Visibility

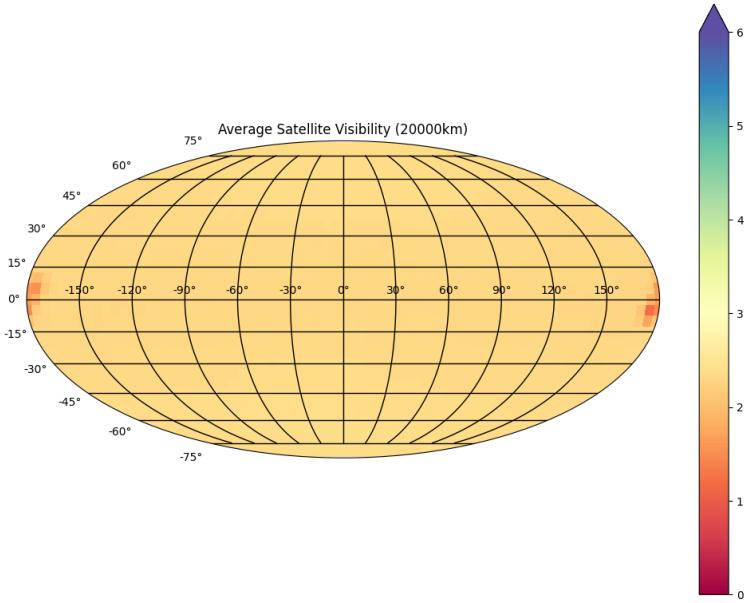


Figure A.17: Average number of satellites visible at $5°$ intervals with no augmentation satellites, in a very high Lunar orbit (altitude = $20\,000\,\mathrm{km}$)

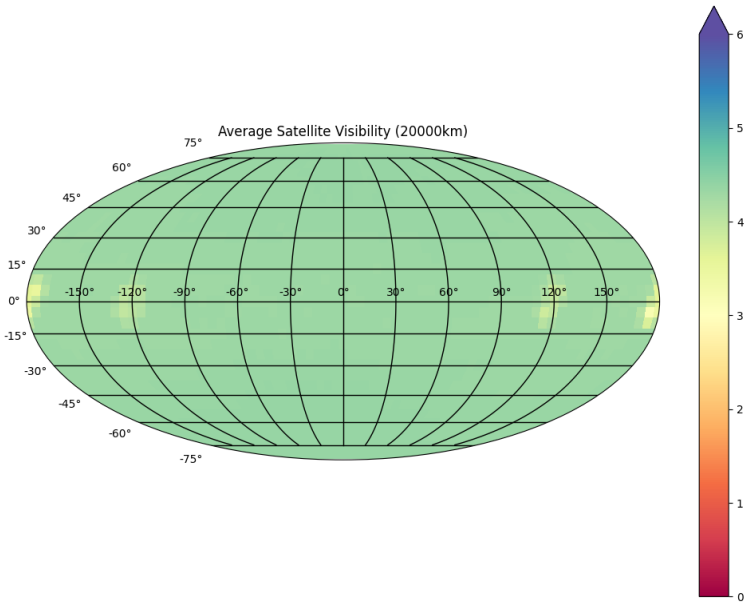


Figure A.18: Average number of satellites visible at $5°$ intervals with augmentation satellites at $L_4$ and $L_5$, in a very high Lunar orbit (altitude = $20\,000\,\mathrm{km}$)

## Average GDOP

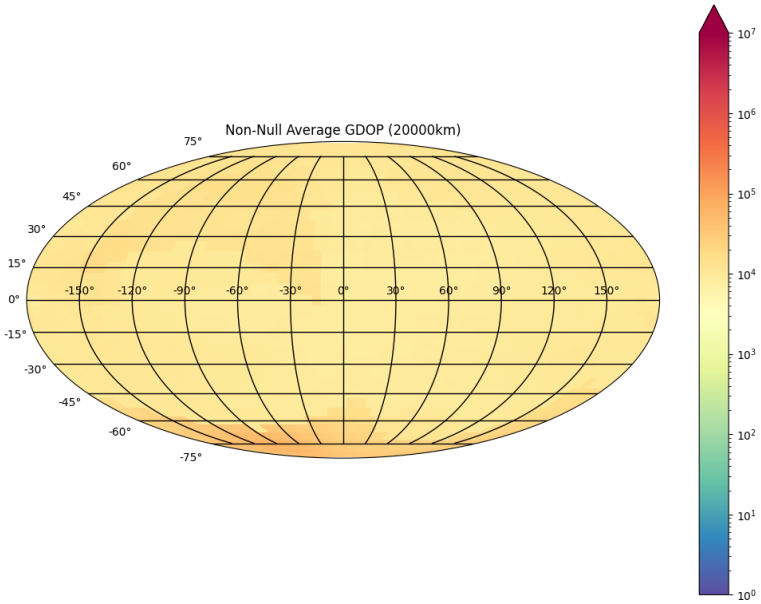


Figure A.19: Average GDOP across $5°$ intervals with no augmentation satellites, in a very high Lunar orbit (altitude = $20\,000\,\mathrm{km}$)

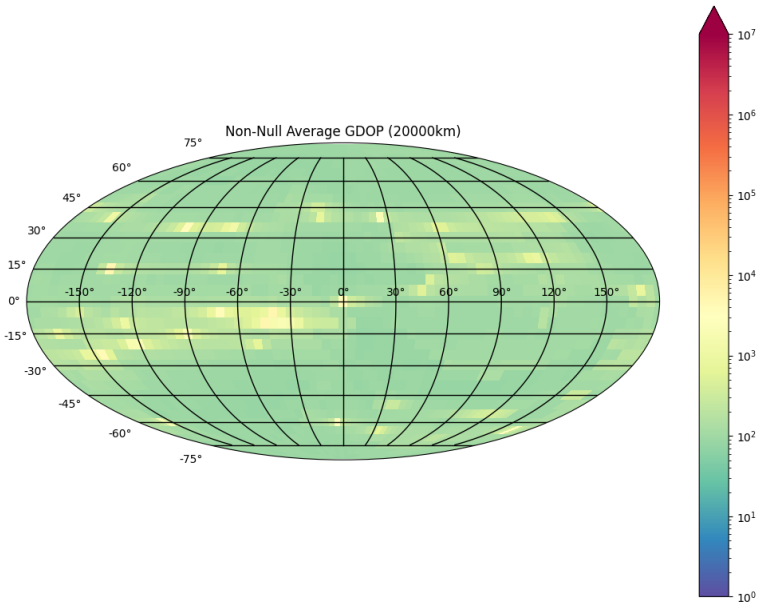


Figure A.20: Average GDOP across $5°$ intervals with augmentation satellites at $L_4$ and $L_5$, in a very high Lunar orbit (altitude = $20\,000\,\mathrm{km}$)